

RESEARCH

Open Access



Exploring the inner hygro-mechanical behaviour of historical panel paintings: a novel approach using digital twins

Riparbelli Lorenzo¹, Mazzanti Paola^{1*}, Helfer Thomas², Manfriani Chiara¹, Uzielli Luca¹, Castelli Ciro³, Santacesaria Andrea³, Ricciardi Luciano³, Rossi Sandra³, Gril Joseph^{4,5} and Fioravanti Marco¹

Abstract

Wooden Panel Paintings (WPPs) stand as invaluable cultural artefacts from the past. These works present an intriguing challenge in understanding their complex mechanical behaviour and ensuring their long-term preservation. The present study assumes as founding paradigm the unicity of each WPP, in terms of its material composition, historical background, physical dimensions, and the specific environmental conditions it has been subjected to over time, and their complex behaviour, which requires the knowledge of both mechanical and materials specificity. These characteristics need to be considered, and studied in-depth for each individual WPP, particularly if the aim is to develop a comprehensive understanding of its individual mechanical behaviour. The study provides new computational models calibrated to reproduce the physical and mechanical behaviour of artworks and acting as their 'digital twins'. The models developed contribute significantly to the understanding of the mechanics of these artworks, including the impact of environmental thermo-hygrometric fluctuations and the role of structural elements such as crossbeams. The results, corroborated by experimental analyses, indicate that environmental variations, both short and long term, exert specific and quantifiable effects on the WPPs, and that the presence of crossbeams significantly influences the distribution of stresses within the panel, particularly affecting the pictorial layers that are often the most susceptible to damage. In this context the generated digital twins serve as an invaluable tool, offering the potential to simulate various risk scenarios or to evaluate the effectiveness of engineered conservation interventions on the WPPs.

Keywords Wooden panel paintings, Conservation, Experimental tests, Numerical modelling, Panel painting deformation tendencies, Paint layer emissivity, Paint layer stiffness

Introduction

Wooden panel paintings (WPP), often centuries old, represent invaluable cultural artifacts that provide insights into the artistic techniques, materials, and cultural contexts of various historical periods. However, their conservation presents a unique set of challenges due to the complexity of their composition and the variability of their responses to environmental conditions [1, 2].

WPPs are systems with a high degree of complexity determined by the variability in material composition—materials with specific physical–mechanical properties and responses to environmental conditions,

*Correspondence:

Mazzanti Paola
paola.mazzanti@unifi.it

¹ DAGRI, Università di Firenze, Florence, Italy

² CEA, DES, IRESNE, DEC, Cadarache, 13108 Saint-Paul-Lez-Durance, France

³ Opificio Delle Pietre Dure, Florence, Italy

⁴ Université Clermont Auvergne, INRAE, PIAF, Clermont-Ferrand, France

⁵ Université Clermont Auvergne, CNRS, Institut Pascal, Clermont-Ferrand, France



© The Author(s) 2024. **Open Access** This article is licensed under a Creative Commons Attribution 4.0 International License, which permits use, sharing, adaptation, distribution and reproduction in any medium or format, as long as you give appropriate credit to the original author(s) and the source, provide a link to the Creative Commons licence, and indicate if changes were made. The images or other third party material in this article are included in the article's Creative Commons licence, unless indicated otherwise in a credit line to the material. If material is not included in the article's Creative Commons licence and your intended use is not permitted by statutory regulation or exceeds the permitted use, you will need to obtain permission directly from the copyright holder. To view a copy of this licence, visit <http://creativecommons.org/licenses/by/4.0/>. The Creative Commons Public Domain Dedication waiver (<http://creativecommons.org/publicdomain/zero/1.0/>) applies to the data made available in this article, unless otherwise stated in a credit line to the data.

the variability of construction techniques and the variability of restoration interventions over time. Despite the wealth of research conducted in this field, a complete understanding of the internal physics of these paintings remains elusive [3].

Previous studies have helped to codify the structure and construction techniques of WPPs, acknowledging the wide range of morphological, instrumental, structural and constructional differences due to different schools and workshops [4, 5]. These studies have also highlighted the inherent variability of wood [6] and how its interaction with the environment can cause mechanical stresses that can lead to permanent deformation, cracking or damage to the paint layers [7–11]. Other studies and monitoring of original works have been also carried out, including the use of optical measurement techniques [12] to correlate deformation fields with the mechanical properties of the paint layers [13–15]. The materials used to construct the WPPs have been characterised, with research focusing on the wooden support [16–18] and the stiffness and vapour and moisture emissivity properties [19–21] of the paint layers [22].

Other research has led to the development of models that capture the dynamics of panel paintings, some of which take into account the complexity of a painting's structure and its responses to environmental variations [23–26]. This body of work is complemented by studies of the interaction between wood and moisture [27], the cracking phenomena of painting layers [10, 28], the response of painted panels to humidity variations [29, 30] and an analysis of the effects of relative humidity cycles [31]. In addition, studies have been carried out on replicas and simulacra to further our knowledge [9, 32, 33]. However, most of these studies have been carried out either on new materials or replicas, as it is often impossible to sample the original WPP components or have access to historical works of art. This has resulted in a limited predictive ability of the behaviour of real materials and or panels that have been subjected to centuries of ageing and reciprocal interactions within the structure.

More recent researches [3, 6] have demonstrated that the main parameters responsible for the hygro-mechanical behaviour of the WPPs are the tree ring orientation of the wooden panels, the stiffness of the ground layers, and the emissivity of the varnishes (and their interactions). However a classificatory model developed has shown that the hygro-mechanical behaviour of the WPPs is hardly predictable if the characteristics of the material making the structure are considered independently, being their interaction that strongly affects such behaviour.

These studies, also established the deformative modalities of the WPPs—observed through tests on original paints and numerical modelling [3] and where the

characteristics of the materials were calibrated on experimental tests [6]. Indeed, these studies, to which we refer also for more detailed methodological information, furnished the fundamental basis for the construction of calibrated models that provided simulated hygro mechanical responses very close to the historical panels. For this reason we can define these models as "digital twins" [34] here intended as virtual replicas of physical objects or systems that facilitate the analysis and simulation of real-world conditions, thereby enabling the prediction of outcomes and the formulation of improvements [4]). Within the context of art conservation, digital twins have surfaced as an instrumental tool for the preservation and study of historical artifacts, including historical panel paintings [5].

In this study, we aim to address the challenges posed by WPPs by exploiting the possibilities offered by digital twins [34, 35]. The proposed approach combines the latest advances in digital technology with traditional art conservation techniques. Specifically, we aim to create digital twins—of selected real WPPs—and use these models to study the internal behaviour of the paintings, with a particular focus on the action at the pictorial layer.

The potential impact of this study goes beyond specific case studies, opening the possibility of a more general analysis of WPPs that will bring important improvements in the understanding of the physics of panel paintings for the definition of more effective conservation strategies.

Materials and methods

A primary objective of this study is to construct calibrated models of historical WPPs. In the following sections we will discuss the fundamental of the adopted numerical modelling, the geometric and numerical modelling of the artworks, the material characterisation of the wooden panels—presented in [6] and merely referenced here—the method for mechanical characterisation of the crossbeams, the approach adopted for a sensitivity study of the parameters involved, and finally, the experimental campaign carried out for validating the results. We will demonstrate how a numerical modeling based on Fick's theory (2.1), applied to three cases of analyzed and modeled paintings (2.2), to which material characteristics derived from experimental tests are applied both for the panels (2.3) and for the crossbeams, is the necessary methodological basis for the construction of digital twins.

Numerical modeling

To simulate moisture diffusion, an isotropic model based on Fick's theory was used, based on its time-dependent form

$$\frac{\partial m_c}{\partial t} = \nabla \bullet \left(\underset{-}{\mathbf{D}} \bullet \nabla m_c \right) \quad (1)$$

Where:

- m_c is the moisture content defined as $m_c = \frac{m-m_0}{m_0}$ where m is the actual mass of wood and m_0 the mass in dry conditions
- $\underset{-}{\mathbf{D}}$ is the tensor of diffusion coefficients, which encapsulates the rate at which moisture diffuses through the wood.
- ∇ represents the gradient operator in vector calculus, used in our study to describe the spatial variation of physical quantities, in our case the moisture content

In this study, the tensor $\underset{-}{\mathbf{D}}$ is simplified to an isotropic form for computational efficiency, as:

$$\underset{-}{\mathbf{D}} = \begin{bmatrix} D_0 \\ D_0 \\ D_0 \end{bmatrix} \quad (2)$$

where D_0 [m^2s^{-1}] is a value of isotropic moisture diffusion.

We used the following boundary condition to model the paint layers emissivity:

$$\frac{q_t}{\rho_0} = E_c \bullet (m_{c,air} - m_{c,sur}) \quad (3)$$

where:

- q_t [$\text{Kg}\cdot\text{s}^{-1}\cdot\text{m}^{-2}$] is the total moisture flux at the paint boundary.
- ρ_0 [$\text{Kg}\cdot\text{m}^{-3}$] is the wood density in dry conditions
- E_c [$\text{m}\cdot\text{s}^{-1}$] is the global moisture effective emissivity of the paint layers.
- $m_{c,air}$ and $m_{c,sur}$ are the wood's equilibrium moisture content corresponding to air humidity and the moisture content immediately below the ground layer, respectively.

We used the following boundary condition to model the rear wooden face of the panel:

$$\frac{q_r}{\rho_0} = E_{c1} \bullet (m_{r,air} - m_{r,sur}) \quad (4)$$

where:

- q_r [$\text{Kg}\cdot\text{s}^{-1}\cdot\text{m}^{-2}$] is the total moisture flux at the paint boundary.
- ρ_0 [$\text{Kg}\cdot\text{m}^{-3}$] is the wood density in dry conditions

- E_{c1} [$\text{m}\cdot\text{s}^{-1}$] is the global moisture effective emissivity of the rear wood surface.
- $m_{r,air}$ and $m_{r,sur}$ are the wood's equilibrium moisture content corresponding to air humidity and the moisture content immediately below the rear face, respectively.

In the computational framework of this study, different types of finite elements were chosen to optimize the accuracy and computational efficiency for various aspects of the analysis, as follows.

First-order hexahedral finite elements were utilized for conducting the hygroscopic analysis, which is critical for capturing the moisture-induced deformations and stresses in the wooden panels.

For the mechanical computations, a more refined approach was adopted. Second-order hexahedral finite elements were used for modelling the panel, offering a higher degree of precision in capturing stress distributions and deformations. In the case of the crossbeams, second-order tetrahedral finite elements were used, providing a balance between computational efficiency and the ability to model complex geometries effectively. It is noteworthy that at each computational step, the hygroscopic field was projected onto the mechanical mesh. The mechanical behaviour of the wood is modelled using a homogeneous orthotropic linear elastic framework, situated in cylindrical coordinates with the pith as the central point. This model also accounts for material shrinkage and swelling in the same cylindrical coordinate system. In terms of computational tools, geometry and discretisation are executed using the open-source software Salome-Meca, developed by Électricité de France (EDF). Simulations are conducted with the open-source solver code_aster [36], while the management of cylindrical coordinates is handled by the open-source software Mfront [37]. The numerical treatment of the contact-friction phenomenon was dealt with a Stabilized Lagrangian formulation following Signorini-Coulomb law [38]; for the Coulomb frictional coefficient a value of 0.4 was chosen [5]. For other specifications and the intrinsic limitation we make reference to ([3, 6]). Due to the presence of non-linear cable elements the model works in large displacements and large rotations.

The results are reported in seven to nine days after the RH step-change of the experiments, until a near equilibrium situation of the moisture in the panels had been reestablished. Two notations are used in the text. The first is used to describe the properties of the wood, denoted by the coordinates R-radial, T-tangential, L-longitudinal, which refer to the anatomical directions of the wood, which are considered here to be analytically cylindrical. The second notation, used to illustrate the results,

is a Cartesian ortho-normal coordinate system. This system is aligned with the plane of the undeformed plank, where the longitudinal direction corresponds to the grain direction and the transverse direction lies on the plane of the paint layer, perpendicular to the longitudinal direction. The notation of the stress characteristics of the crossbeams is based on the notation of beam elements used in solid mechanics.

The analysed WPPs and their geometrical modeling.

In this study, three historical paintings have been subjected to a careful analysis with the primary objective of exploring the wide range of behaviour that they can

exhibit, based on the previous studies [3, 6]. The selection of these WPPs, as the focus of the study, was guided by their significant diversity in observed behaviour, as well as the notable differences in material characteristics, structural elements, and construction methods.

Table 1 shows a brief qualitative characterization of these three WPPs. Such characterization is fundamental for understanding the substantial differences among them and for identifying the unique challenges and opportunities that each of them may offer for conservation and research in the field of wooden panel painting. A very important distinctiveness of panel paintings is their deformation behaviour. A transient deformation may

Table 1 Paintings chosen for this study and their characteristics, the (non) monotonous character of the behavior refers to the response to a step humidity change, called (non) flying wood. More information on this topic are present in [3]

| # | WPP | Dimensions | Main Characteristics |
|---|-------------------------------------------------------------------------------------------------------------------------------------------|-------------------------------------------------------------------------------------------------------------------------------------------------------|-------------------------------------------------------------------------------------------------------------------------------------------------------------------------------------------------------------------------------------------------------------------------------------|
| 1 | <p><i>Madonna with Child</i></p>  | <p>530 × 900 × 14 mm Panel in Poplar (<i>Populus alba L.</i>) Crossbeams in chestnut (<i>Castanea sativa Mill.</i>)</p> | <ul style="list-style-type: none"> • Behavior: non monotonous • Behavior with insulated front: monotonous • Medium Paint Layer Stiffness • Medium Paint Emissivity • Low rear Emissivity • 40 mm distant from the pith |
| 4 | <p><i>Madonna with Child, Saint John and monk</i></p>  | <p>645 × 775 × 23 mm Panel in Poplar (<i>Populus alba L.</i>) Crossbeams in chestnut (<i>Castanea sativa Mill.</i>)</p> | <ul style="list-style-type: none"> • Behavior: monotonous • Behavior with insulated front: monotonous • High Paint Layer Stiffness • Medium Paint Emissivity • Medium rear Emissivity • 20 mm distant from the pith |
| 5 | <p><i>Crucifixion with Madonna and Saint John</i></p>  | <p>655 × 855 × 30 mm Panel in Poplar (<i>Populus alba L.</i>) Crossbeams in chestnut (<i>Castanea sativa Mill.</i>)</p> | <ul style="list-style-type: none"> • Behavior: non monotonous • Behavior with insulated front: non monotonous • Medium Paint Layer Stiffness • Low Paint Emissivity • Low rear Emissivity • 50 mm distant from the pith |

arise as a result of variations in Relative Humidity (RH). This phenomenon is attributable to the hygroscopic disparity between the two surfaces of the panel painting: the exposed wood on the rear and the painted facade on the front, compounded by the rigidity of the paint layer. Characterizing this transient phase is the emergence of asymmetric moisture gradients throughout the panel's thickness. Such gradients can induce a distinctive deformation, commonly referred to as 'flying wood', wherein the panel exhibits a non-monotonic pattern of cupping and deflection. Conversely, in the 'non-flying wood' scenario, the panel's response to moisture changes is characterized by a monotonic behavior.

The geometric modelling of the panels was carried out through the digital construction of three-dimensional bodies, consistent with the dimensions shown in Table 1. These bodies were partitioned into 30 layers in thickness to accurately capture moisture gradients. Also the crossbeams were digitally reconstructed as three-dimensional bodies following accurate measurements. These panels, restored during previous interventions at OPD (Opificio delle Pietre Dure) [39] are characterized by the following significant features:

- Relative displacements between the crossbeam and the panel in the plane of the panel are permitted.
- The connections on the panels are as described in [39, 40].
- The boards forming the panels are restored and well-glued along the edges, allowing for global distortions of the panel, rather than independent distortion of individual boards.
- The paint layers are well-adhered to the wooden panel.

Table 2 shows the geometric models of the three WPPs considered in this study—WPP1, WPP4, and WPP5—alongside with two additional models, Sensitivity1 and Sensitivity2, added for the sensitivity studies (see "Sensitivity study" section). Symmetry constraints are imposed on the panels and on the crossbeams of the sensitivity study models to save degrees of freedom for the numerical solution, and to ensure that the results are meaningful and not influenced by edge effects.

The red circles show the locations from which the results reported in "Digital Twins: Validation" section have been extracted from the full fields of the time dependent results in the whole mesh discretization. The rationale behind the selection of these points is that they are centrally located on the panel and equidistant from the two crossbeams. This strategic positioning minimises the influence of local effects and force concentrations, thereby facilitating the acquisition of results that

are as generalisable as possible. This choice is rooted in the understanding that the central regions of the panel are less susceptible to localized mechanical behaviours that may arise due to the presence of crossbeams, anchor points, or friction zones. By selecting points that are equidistant from these structural elements, the data extracted is less likely to be skewed by such localised phenomena.

A special modelling technique has been used to approximate the actual connection between the crossbeam and the panel, as referenced in [40]. As shown in Fig. 1, two beam elements have been inserted into the hole at the level of the crossbeam's outer surface. The beam element aligned with the direction of the crossbeam has negligible stiffness compared to the crossbeam itself, to avoid any undue flexural stiffening of the crossbeam. Conversely, the beam element in the perpendicular direction is highly rigid. The constraint between these elements and the wood of the crossbeam restricts translational movements only. For the purposes of this experiment, to eliminate the variable stiffness and forces of the springs, they were fully tightened prior to testing. This resulted in a rigid, non-extendable behaviour, transmitting a constant and quantified pre-load of 60 N per spring between the panel and the crossbeams. The spring element was thus modelled as a non-linear cable-type element. It spatially extends between the two aforementioned beam elements and the attachment point of the wooden support glued to the panel. The element has a circular cross-section with a diameter of 10 mm and carries a pre-load of 60 N.

Material properties of the wooden supports

The material properties utilised in the subsequent discussion have been obtained through the inverse engineering processes described in [6], and shown in Table 3. A simplification made herein is the extension of material properties computed for individual boards to all other boards forming the same panel. This is due to the inherent limitation of using the Deformometric Kit (DK)[41], which reads a single cupping angle derived from the combined cupping of all the wood sections included between the two points on which DK's columns are applied on the wood.

Material properties of the crossbeams

The study of the flexural stiffness of the crossbeams is not trivial, because they feature several holes where the anchoring devices are located. Since the assumptions for the application of Euler's beam theory are not met, we chose to carry out several bending test using an optimisation procedure aiming at minimising the difference between experimental and numerical results, based on [5, 26].

Table 2 Geometry, discretization (mesh) and information about the modelling

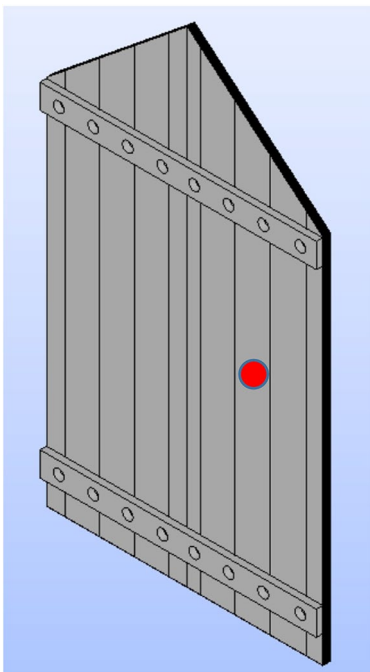
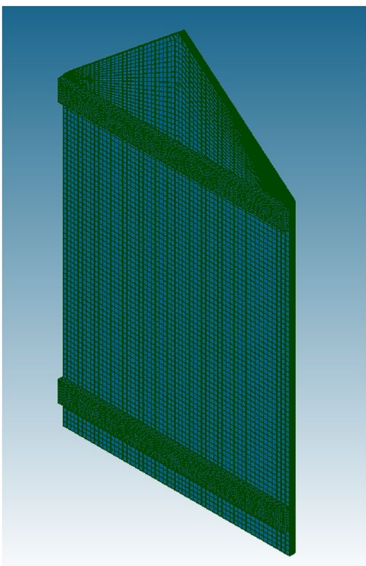
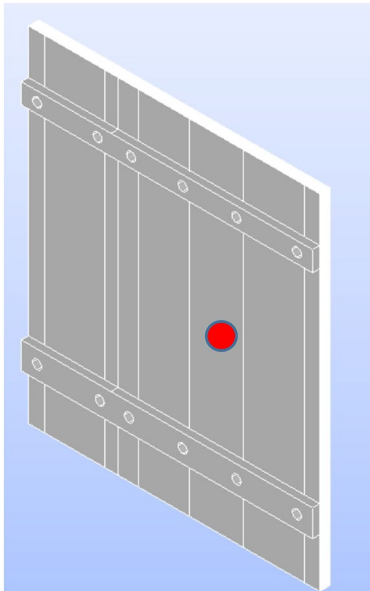
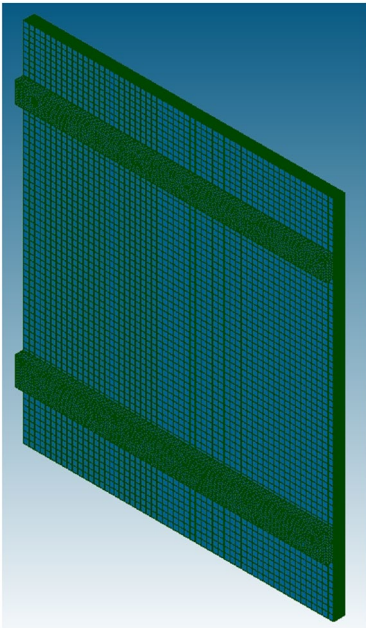
| WPP | Model geometry | Discretization | Main characteristics. Type and number of elements |
|-----|-------------------------------------------------------------------------------------|--------------------------------------------------------------------------------------|---------------------------------------------------------------------------------------------|
| 1 |  |  | <ul style="list-style-type: none"> • 85,680 Hexahedrons, 30,805 Tetrahedrons |
| 4 |  |  | <ul style="list-style-type: none"> • 63,954 Hexahedrons, 60,085 Tetrahedrons |

Table 2 (continued)

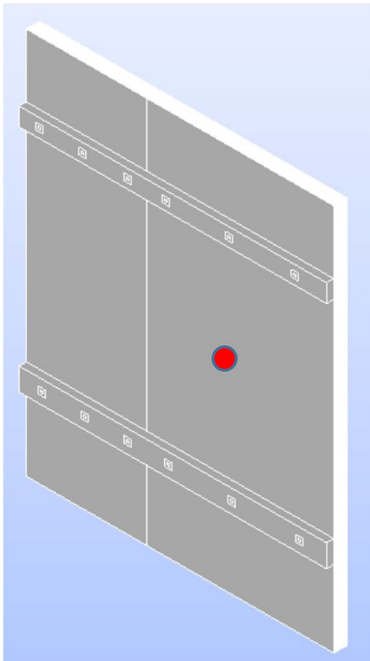
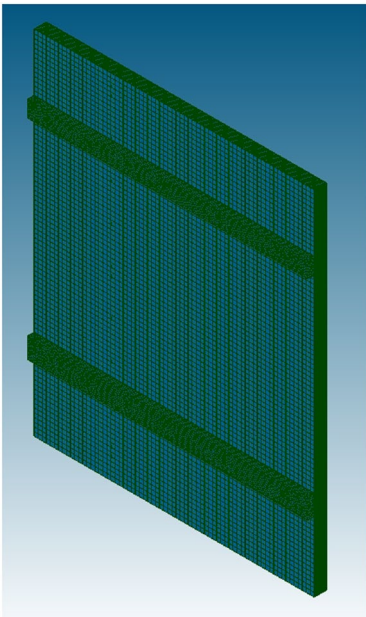
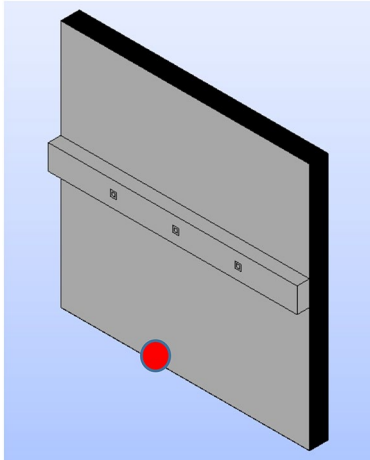
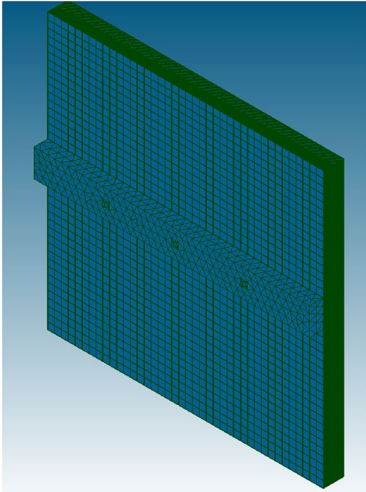
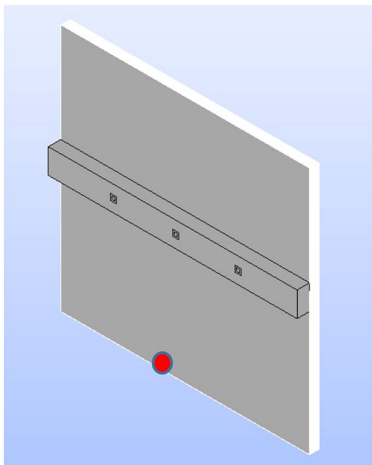
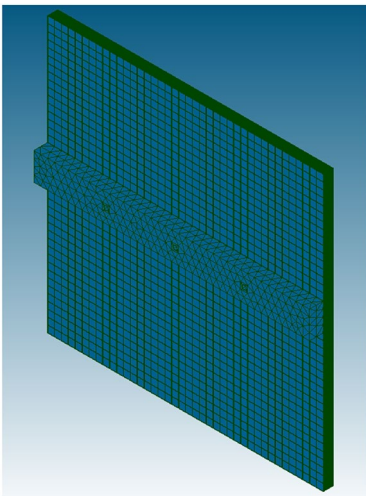
| WPP | Model geometry | Discretization | Main characteristics. Type and number of elements |
|--------------|-------------------------------------------------------------------------------------|--------------------------------------------------------------------------------------|---------------------------------------------------------------------------------------------------------------------------------------------------------------------|
| 5 |  |  | <ul style="list-style-type: none"> • 100,878 Hexahedrons, 45,327 Tetrahedrons |
| Sensitivity1 |  |  | <ul style="list-style-type: none"> • 51,500 Hexahedrons, 1855 Tetrahedrons • Panel 15 × 400 × 400 mm • Crossbeam: 20 × 40 × 400 mm |

Table 2 (continued)

| WPP | Model geometry | Discretization | Main characteristics. Type and number of elements |
|--------------|-----------------------------------------------------------------------------------|------------------------------------------------------------------------------------|---------------------------------------------------------------------------------------------------------------------------------------------------------------------|
| Sensitivity2 |  |  | <ul style="list-style-type: none"> • 51,500 Hexahedrons, 1855 Tetrahedrons • Panel 30 × 400 × 400 mm • Crossbeam: 20 × 40 × 400 mm |

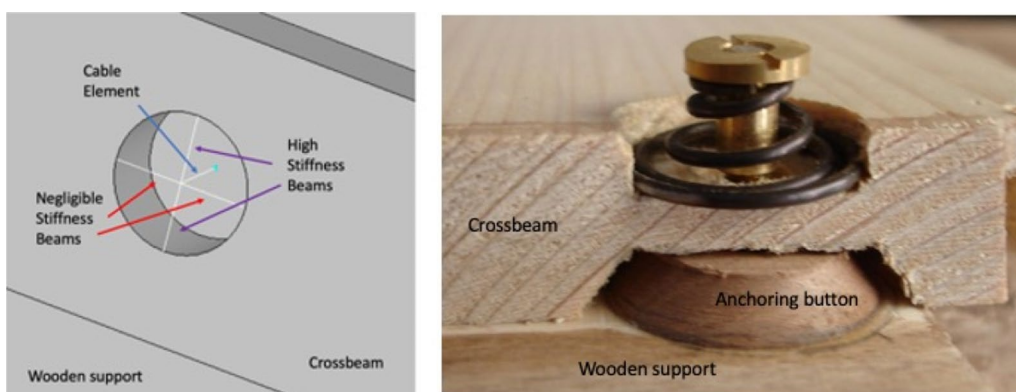


Fig. 1 Modeling one of the connections between crossbeam and panel on the left, and mock-up section of the related restoration technique at the OPD on the right

Table 3 Summary of the computed hydro-mechanical values for the studied WPPs

| | D_0 [$m^2 \cdot s^{-1}$] | E_p [MPa] | E_c [$m \cdot s^{-1}$] | E_{c1} [$m \cdot s^{-1}$] | X | Y |
|------|------------------------------|-------------|----------------------------|-------------------------------|------|------|
| WPP1 | $4.0 \cdot 10^{-10}$ | 1506 | $7.5 \cdot 10^{-08}$ | $9.0 \cdot 10^{-08}$ | 0.62 | 0.82 |
| WPP4 | $6.0 \cdot 10^{-10}$ | 10,500 | $3.0 \cdot 10^{-08}$ | $1.8 \cdot 10^{-07}$ | 2.05 | 1.5 |
| WPP5 | $1.1 \cdot 10^{-09}$ | 1952 | $1.0 \cdot 10^{-10}$ | $2.6 \cdot 10^{-07}$ | 1.29 | 0.55 |

Do Diffusion coeff., E_c Paint layers face emissivity, E_{c1} Back face emissivity, E_p Rigidity of paint layers, X and Y corrective coefficients for shrinking/swelling and wood compliance

The crossbeams were subjected to a three-point bending test, largely in accordance with the UNI EN 408 European standard, although some modifications to the geometry of the load application points were necessary. Each crossbeam was sequentially loaded with dead loads

applied on three selected points: one centrally positioned between the supports and two equally spaced on either side. The loading was incrementally applied in steps of approximately 50 N, up to a load of around 400 N. Deflections were quantified using three digital gauges

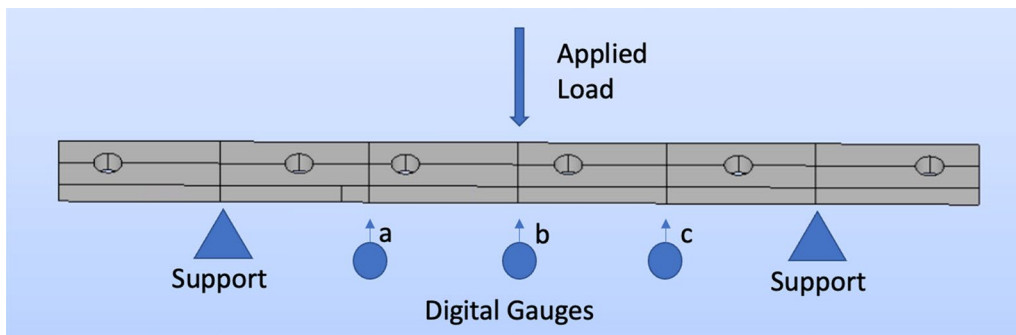


Fig. 2 Schema of the bending test for the crossbeams, and specific modelling of the high crossbeam of WPP4. The arrow at the top indicate the sequential load application, ranging from zero to 400 N, at each of the three designated locations. The two lateral arrows beneath the beam signify the constraint reaction forces exerted by the supports. Symbols located under the beam, labelled as ‘a’, ‘b’, and ‘c’, correspond to the digital gauges used for measuring the vertical deflections at the respective locations

(Mitutoyo Absolute ID-U1025), which have a resolution of 0.01 mm and an accuracy of 0.02 mm. These gauges were strategically positioned beneath the loading points. The schematic representation of the bending tests conducted on the crossbeams is shown in Fig. 2.

To perform the optimization a cost functional J was introduced, dependent on c , vector of the n parameters to be identified:

$$J(c) = \|d - d_{exp}\| \tag{5}$$

where d are the numerically calculated reactions in the position of the load cells, d_{exp} are the corresponding mechanical reactions experimentally determined and $\|\cdot\|$ is a norm on L , space of the observable values. The inverse identification is a minimization of the cost functional $J(c)$, where we want to find $c^* \in O$, closed convex of \mathbb{R}^n :

$$J(c^*) = \min_{c \in O} J(c) \tag{6}$$

The minimisation was performed by means of a technical solution based on a genetic algorithm followed by a Nelder Mead-type algorithm([6]).

A W coefficient that multiplies the fourth-order compliance tensor in the following way, was optimized:

$$S_{ij}^* = W^{-1} \bullet S_{ij}^0 = \begin{pmatrix} W^{-1}S_{11}^0 & W^{-1}S_{12}^0 & W^{-1}S_{13}^0 & 0 & 0 & 0 \\ W^{-1}S_{12}^0 & W^{-1}S_{22}^0 & W^{-1}S_{23}^0 & 0 & 0 & 0 \\ W^{-1}S_{13}^0 & W^{-1}S_{23}^0 & W^{-1}S_{33}^0 & 0 & 0 & 0 \\ 0 & 0 & 0 & W^{-1}S_{44}^0 & 0 & 0 \\ 0 & 0 & 0 & 0 & W^{-1}S_{55}^0 & 0 \\ 0 & 0 & 0 & 0 & 0 & W^{-1}S_{66}^0 \end{pmatrix} \tag{7}$$

where S_{ij}^* is the optimized compliance tensor, S_{ij}^0 the components of the compliance matrix estimated based on the values of Table 4 ([42, 43]) for each chestnut crossbeam:

Sensitivity study

In order to gain a more nuanced understanding of the behaviour of the digital twins of the historical WPPs and their difference in behaviour with and without crossbeams, this study was supported with a sensitivity analysis. The aim being to elucidate how various variables at play affect the overall behaviour of an artwork, the variable are taken from the material properties of WPP3 [6] to render the sensitivity study independent from the other specific cases, while using real properties of an actual historic WPP. This was achieved by subjecting a panel, stiffened by crossbeams and not stiffened, to a step humidity change of $\Delta m_c = -0.62\%$ (corresponding to a variation of RH 51–60%, [6],) while imposing the following parameters:

- a) Two different panel thicknesses, thereby affecting both the stiffness ratio between the crossbeam and the panel as well as the hygroscopic equilibration times.
- b) Two limiting hygroscopic behaviour conditions; the first where the emissivity of the front and back

Table 4 Initial material properties for the optimization process of the crossbeams

| E_L | E_R | E_T | ν_{LR} | ν_{RT} | ν_{LT} | G_{LR} | G_{RT} | G_{LT} |
|----------|---------|---------|------------|------------|------------|----------|----------|----------|
| 8500 MPa | 800 MPa | 800 MPa | 0.31 | 0.71 | 0.31 | 1500 MPa | 65 MPa | 1500 MPa |

surfaces are essentially comparable, and the second where the emissivity of the back surface is significantly larger than that of the front (by two orders of magnitude), resulting in nearly symmetrical and entirely asymmetrical gradients, respectively.

- c) Three distinct values for the stiffness of the paint layers—low, medium, and high stiffness—based on the evidence provided by [6].
- d) All the boards are cut 50 mm from the pith from the side of the paint layers.
- e) In the initial state of the analysis the panels are not presenting coactions in terms of stress and strains induced by moisture.

Table 5 shows the material properties used for the sensitivity study:

Experimental tests

WPP1, WPP4 and WPP5 were instrumented with a DK, as described in [3, 6], and exposed to controlled step changes in Relative Humidity (RH). A climatic chamber was constructed within the Opificio delle Pietre Dure restoration laboratories. Humidity control was achieved through a Preservatech miniOne humidifier, complemented by a ventilation system consisting of six fans and the humidifier’s inherent operational capacity. Real-time monitoring of RH and temperature (T) was conducted using URT Smart CEAM LoRa-C sensors, with an accuracy of $\pm 2\%$ for RH and $\pm 0.5\text{ }^\circ\text{C}$ for temperature. Data points were captured at 15-min intervals and

continuously aggregated via the CEAM CWS software, a web-cloud-IoT-based integrated platform designed for monitoring, control, and collaborative management. The panel paintings were positioned vertically within the climatic chamber, and the contact surfaces were coated with Polytetrafluoroethylene (PTFE) to mitigate frictional effects. The humidity steps were between 51 and 60% and the temperature was constant at 20 °C [Fig. 3]. The panel paintings were left at least 35 days in a equilibrated climate condition.

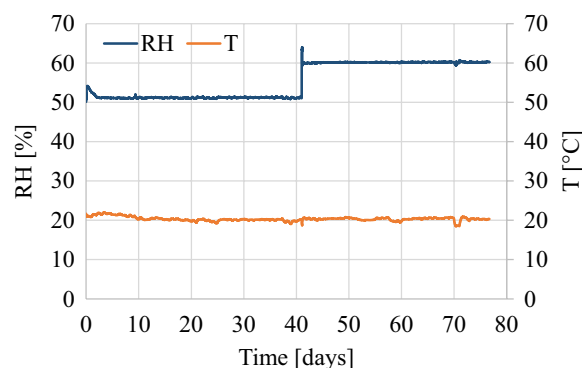


Fig. 3 The time history of the climatic condition variation the panel paintings underwent. The RH varied from 51 to 60%. The T was non controlled inside the box and depended from the air conditioning of the room, which was 20 °C

Table 5 Material properties and thickness chosen for the sensitivity study

| | D_0 [$\text{m}^2\cdot\text{s}^{-1}$] | E_p [MPa] | E_c [$\text{m}\cdot\text{s}^{-1}$] | E_{c1} [$\text{m}\cdot\text{s}^{-1}$] | X | Y | Thickness [mm] |
|--------|------------------------------------------|-------------|----------------------------------------|-------------------------------------------|-----|------|----------------|
| Test1 | $1.6 \cdot 10^{-8}$ | 100 | $4.3 \cdot 10^{-8}$ | $5.0 \cdot 10^{-8}$ | 0.8 | 0.93 | 30 |
| Test2 | $1.6 \cdot 10^{-8}$ | 1000 | $4.3 \cdot 10^{-8}$ | $5.0 \cdot 10^{-8}$ | 0.8 | 0.93 | 30 |
| Test3 | $1.6 \cdot 10^{-8}$ | 10,000 | $4.3 \cdot 10^{-8}$ | $5.0 \cdot 10^{-8}$ | 0.8 | 0.93 | 30 |
| Test4 | $1.6 \cdot 10^{-8}$ | 100 | $4.3 \cdot 10^{-10}$ | $5.0 \cdot 10^{-8}$ | 0.8 | 0.93 | 30 |
| Test5 | $1.6 \cdot 10^{-8}$ | 1000 | $4.3 \cdot 10^{-10}$ | $5.0 \cdot 10^{-8}$ | 0.8 | 0.93 | 30 |
| Test6 | $1.6 \cdot 10^{-8}$ | 10,000 | $4.3 \cdot 10^{-10}$ | $5.0 \cdot 10^{-8}$ | 0.8 | 0.93 | 30 |
| Test7 | $1.6 \cdot 10^{-8}$ | 100 | $4.3 \cdot 10^{-8}$ | $5.0 \cdot 10^{-8}$ | 0.8 | 0.93 | 15 |
| Test8 | $1.6 \cdot 10^{-8}$ | 1000 | $4.3 \cdot 10^{-8}$ | $5.0 \cdot 10^{-8}$ | 0.8 | 0.93 | 15 |
| Test9 | $1.6 \cdot 10^{-8}$ | 10,000 | $4.3 \cdot 10^{-8}$ | $5.0 \cdot 10^{-8}$ | 0.8 | 0.93 | 15 |
| Test10 | $1.6 \cdot 10^{-8}$ | 100 | $4.3 \cdot 10^{-10}$ | $5.0 \cdot 10^{-8}$ | 0.8 | 0.93 | 15 |
| Test11 | $1.6 \cdot 10^{-8}$ | 1000 | $4.3 \cdot 10^{-10}$ | $5.0 \cdot 10^{-8}$ | 0.8 | 0.93 | 15 |
| Test12 | $1.6 \cdot 10^{-8}$ | 10,000 | $4.3 \cdot 10^{-10}$ | $5.0 \cdot 10^{-8}$ | 0.8 | 0.93 | 15 |

Results

In this section is reported a detailed analysis of the experimental and computational findings. It begins with a comprehensive exploration of the immediate effects of environmental changes on WPPs, as observed in our experiments. This is followed by a discussion of the sensitivity analysis outcomes, revealing how various factors impact the structural integrity of the panels. Subsequent sections delve into the implications of these findings, particularly focusing on the stresses and deformations experienced by the panels under different conditions.

Experimental tests on historical paintings

In this section, we present the values of the cupping angle variation with time, that is observed for WPP1, WPP4 and WPP5 with the crossbeams mounted on, with the aim of rendering the data compatible for comparative analysis (Fig. 4). To facilitate a comparative evaluation of the results obtained from the three WPPs, the data have been normalised with respect to the span of the DKs of 300 mm.

Such data are found to be in alignment with the results presented in [3], with the crossbeams serving to mitigate the cupping deformations observed in unrestrained panels. This is generally the primary objective of crossbeam systems used in the conservation of these artworks. In the plot depicting the cupping angle, abrupt scattering are discernible, attributable to transitions between static and dynamic friction between the crossbeams and the panel boards. Thus, the sliding motion of the crossbeam over the panel is constrained by frictional forces. When the tangential frictional force surpasses the threshold limit of static friction, a brief, abrupt shift occurs, transitioning into a state of dynamic friction. This phenomenon is not merely a trivial observation but rather an essential aspect that adds another layer of complexity to the mechanical behaviour of WPPs. These transitions between static and dynamic friction are indicative of the intricate interplay between the crossbeams and the panel boards, particularly in terms of stress distribution and deformation characteristics.

Sensitivity study

In this section, we present a selective portion of the sensitivity study (Test4, Test5, Test6 of Table 5), confining our focus to panels characterised by considerable thickness and pronounced hygroscopic asymmetry in their gradients. We have opted for this approach, deferring the complete results to the supplementary material, based on the observation that, despite significant data variations across different cases, they invariably conform to the same underlying physical dynamics that are of interest

in this study. How stresses and deformations evolve over time across the thickness in control segments of panels was examined, both in the absence and presence of crossbeams. Finally, the differences in stress and deformation profiles as plotted across the thickness of the artworks were delineated. In each diagram of Figs. 5, 6, and 7, we can observe the thickness of the panel, indicated by a darker grid pattern in correspondence with the paint layers. Overlaid on this there are diagrams depicting the characteristics of interest—be it moisture content, stress, strain, etc. These are repeated adjacently with a temporal distance of 24 h for the first nine days of climatic variation, each corresponding to a specific time point. This method of presentation serves multiple purposes. Firstly, it allows for a more nuanced understanding of how these characteristics evolve over time, particularly in response to environmental thermo-hygro-metric variations. Secondly, it provides a comprehensive visual representation that facilitates the comparison of these evolving characteristics against the constant physical structure of the artwork, specifically the panel and the paint layers. In [Annex](#) is present an explanation on how to read the following plots (Fig. 15).

We can generally observe that the step change in humidity induces an initial peak of stress on the back face of the panel (in the case of a humidity decrease), which tends to significantly diminish over time. This phenomenon is attributable to the initial deformation tendency of the topmost wood layers, which are immediately affected by the concentrated hygroscopic gradient. This effect is not counterbalanced by the layers just beneath them, as these are not yet sufficiently influenced by the moisture gradient. In contrast, we note an opposite behaviour in the paint layers, where stresses substantially increase over time before stabilising at elevated levels upon the maintenance of the step impulse. This behaviour thus signifies a significant interaction between the wood and the paint layers, attributable to the different hygroscopic properties of the two materials. With respect to deformations, we observe that, except for the initial moments of the transient phase, the sections are consistently contracted at every point, with the maximum value occurring on the back side of the panel and the minimum on the paint layers. The effect of the crossbeams leads to a reduction in deformations on the back and an increase in those on the front face, consequently resulting in a decrease in the panel's cupping angle. It is crucial to observe that the point to point variation in deformational behaviour between the two distinct physical states—the unrestrained panel and the panel reinforced by crossbeams—follows a linear trajectory. This trajectory exhibits a minor asymmetry relative to the zero point, an asymmetry that amplifies with the increase in the

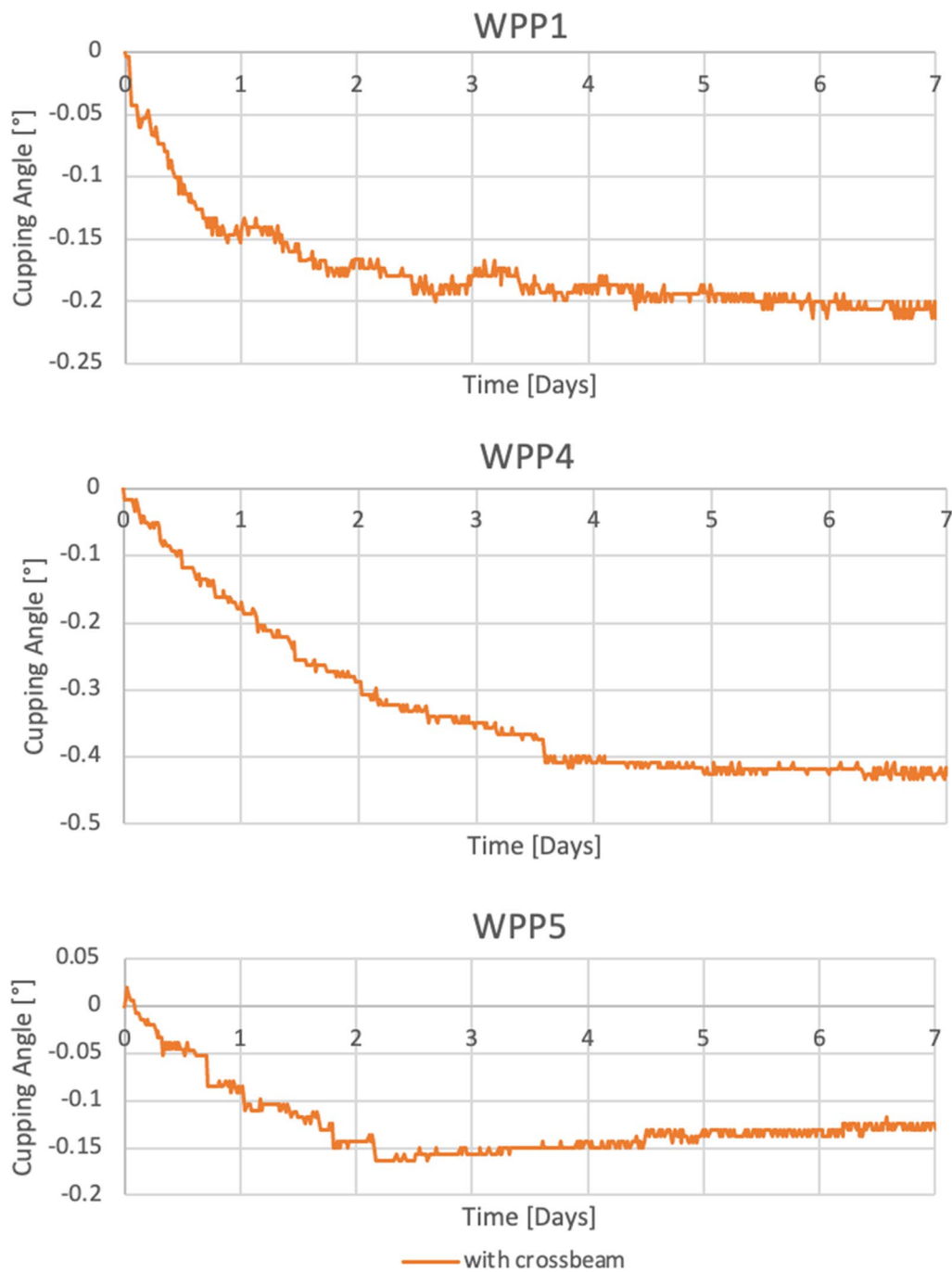


Fig. 4 Measured cupping angle for the 3 paintings with crossbeams for the step humidity change

mechanical rigidity of the paint layers. In relation to the corresponding variation in stress distribution, the phenomenon precisely manifests as a piecewise linear function at the juncture of material discontinuity (wooden support and paint layers).

Stiffness of the crossbeams

Herein is presented the outcome of one of the bending tests conducted on the crossbars, specifically focusing on the upper crossbar of WPP4 (Fig. 8), along with the results of the optimisation process that enabled the determination of the stiffness multiplier for all the crossbars of the studied paintings, in Table 6.

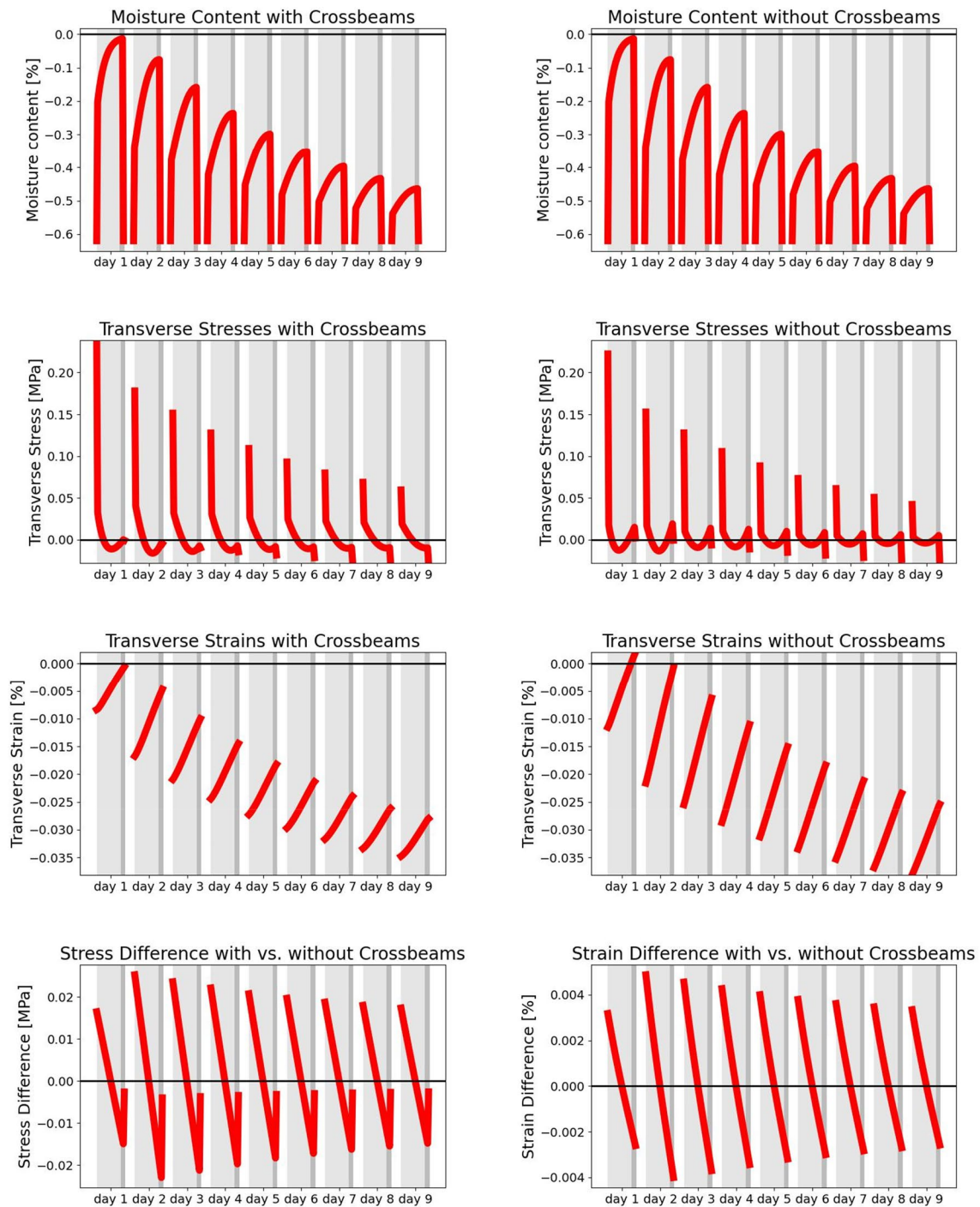


Fig. 5 Results of Test4 in terms of Moisture content variation from the previous equilibrium state, stresses and strains in the plane of the panel perpendicular to the grain in the cross section for the panel with and without the crossbeams, and the difference in stress and strains between the two states. As the gradient of moisture content in the thickness of the panel is the driver of the phenomenon it is repeated two times in the first row to assure to the reader a vertical responsiveness on both columns and the fact that the distribution of moisture is exactly the same at each timestep for both cases with and without crossbeams

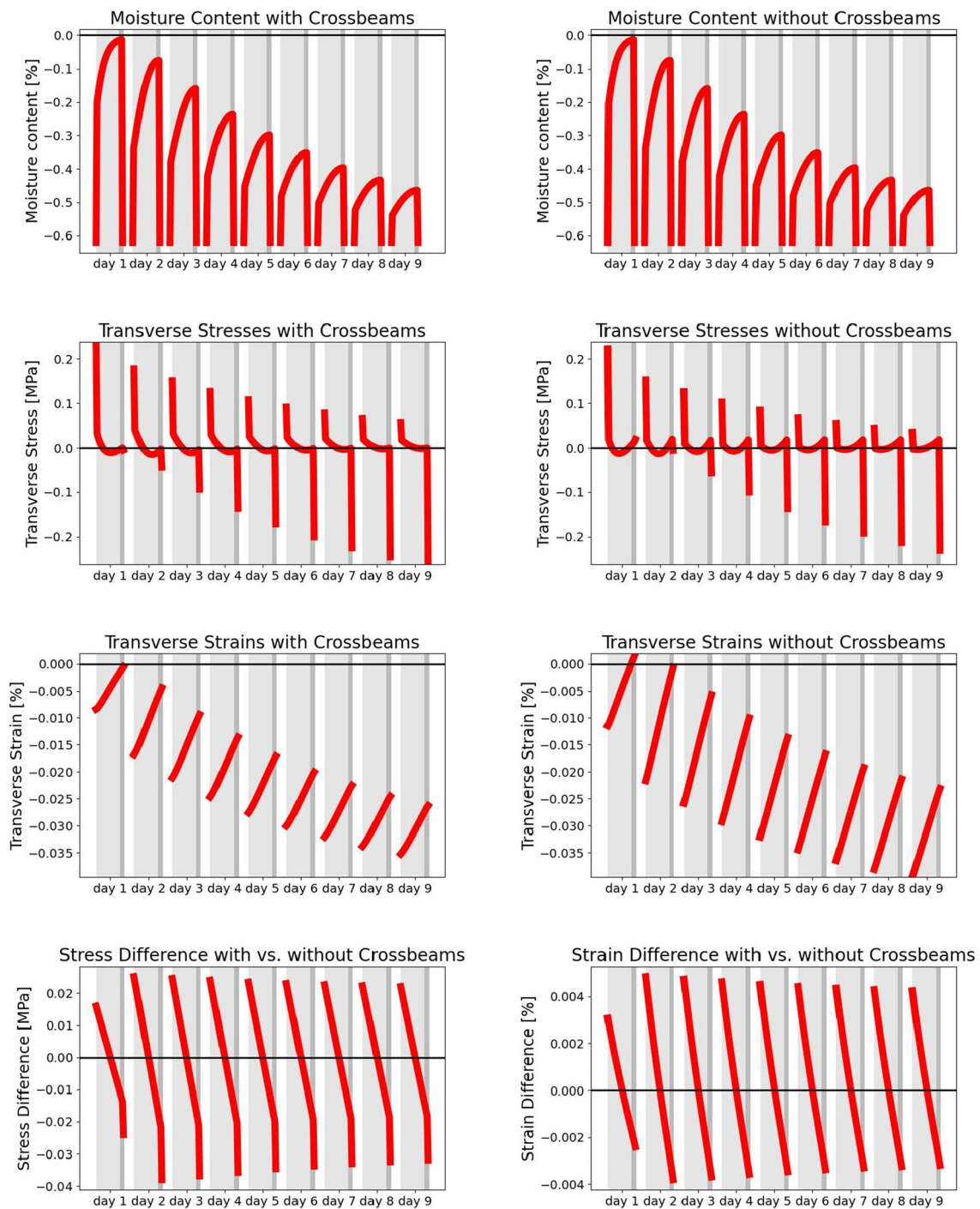


Fig. 6 Results of Test5 in terms of Moisture content variation from the previous equilibrium state, stresses and strains in the plane of the panel perpendicular to the grain in the cross section for the panel with and without the crossbeams, and the difference in stress and strains between the two states. As the gradient of moisture content in the thickness of the panel is the driver of the phenomenon it is repeated two times in the first row to assure to the reader a vertical response on both columns and the fact that the distribution of moisture is exactly the same at each timestep for both cases with and without crossbeams

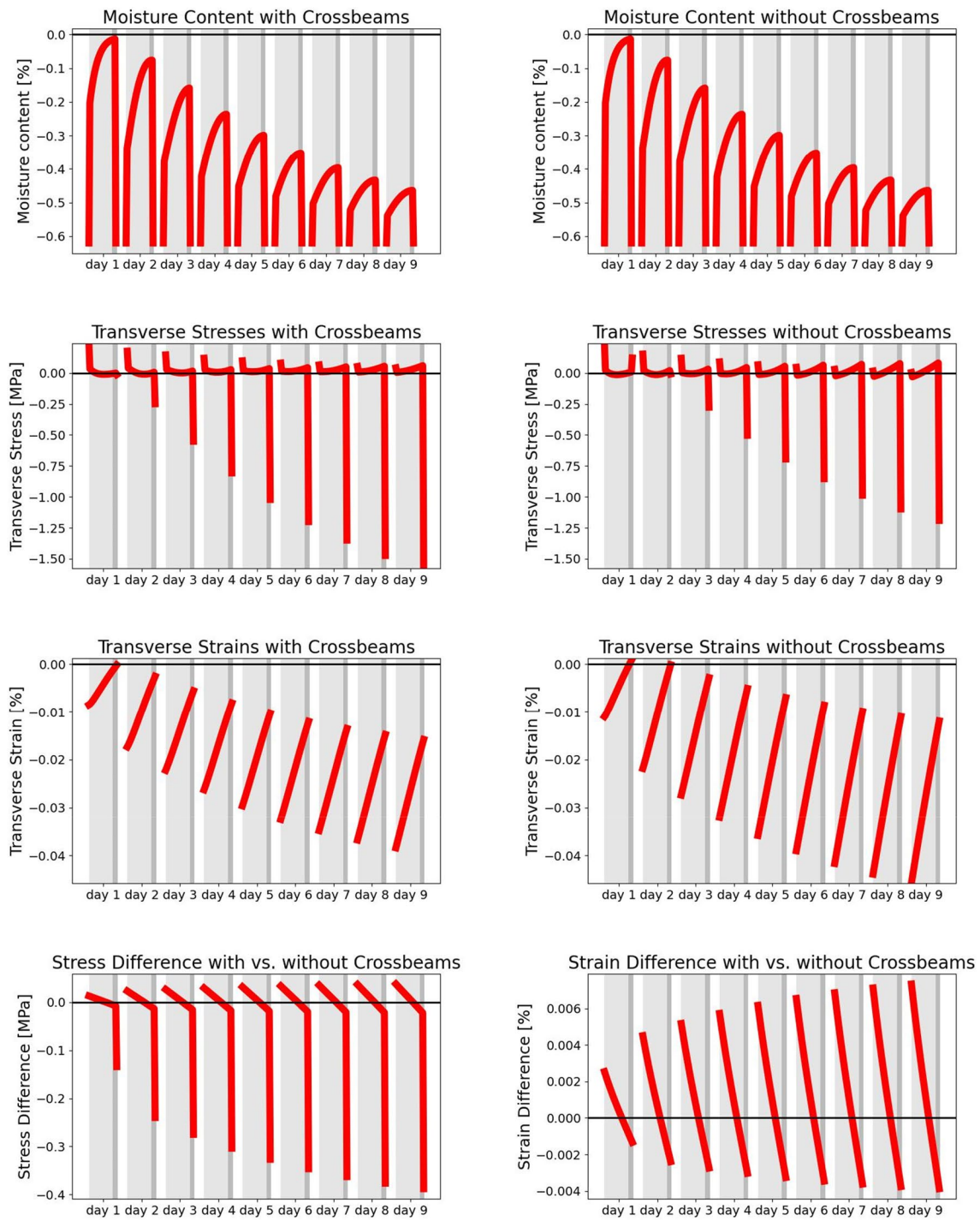


Fig. 7 Results of Test6 in terms of Moisture content variation from the previous equilibrium state, stresses and strains in the plane of the panel perpendicular to the grain in the cross section for the panel with and without the crossbeams, and the difference in stress and strains between the two states. As the gradient of moisture content in the thickness of the panel is the driver of the phenomenon it is repeated two times in the first row to assure to the reader a vertical response on both columns and the fact that the distribution of moisture is exactly the same at each timestep for both cases with and without crossbeams

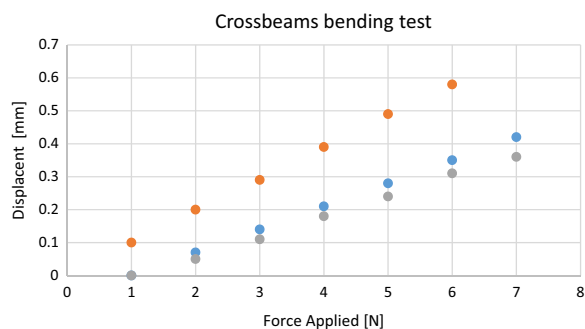


Fig. 8 Bending tests results of the higher crossbeam of WPP4. Where, with reference to Fig. 2, the vertical displacements of the dial indicators (grey—a, orange—b, blue—c) are represented as the central load imposed on the crossbeam varies

Table 6 Results of the stiffness optimization for all the crossbeams of WPP1, WPP4, WPP5; W represents the multiplier of the compliance tensor

| WPP—Crossbeam | W |
|---------------|------|
| WPP1—High | 0.74 |
| WPP1—Low | 0.89 |
| WPP4—High | 1.12 |
| WPP4—Low | 1.01 |
| WPP5—High | 0.92 |
| WPP5—Low | 0.90 |

Digital twins: validation

In Fig. 9, we can observe a comparative analysis between the experimental and simulated results pertaining to the two conditions—panels with and without crossbeams. It is evident that the general form of the curve describing the cupping angle remains substantially consistent across both conditions. In this context, the role of the crossbeams serves merely as a mitigator of cupping deformations. As for the simulated results, it is noteworthy that the material parameters were calibrated under the condition without crossbeams [3]. Therefore, it is expected that the numerical outcomes would closely align with the experimental data. The misalignment discrepancy of WPP5 has already been discussed in [6] for the case without crossbeams. However, the experimental case with crossbeams is very consistent with the analysis, thereby confirming the characterization values obtained in [6]. The high degree of congruence between the numerical and experimental results in the case with crossbeams show the efficacy of the modelling approach chosen (Figs. 10 and 11).

Digital twins: results

In this section, we present the results pertaining to WPP1 (Fig. 10), WPP4 (Fig. 11) and WPP5 (Fig. 12), focusing on the comparison between deformations and stresses, with and without crossbeams. This analysis uses the same methodological framework used in the sensitivity study. The aim is to elucidate the interplay between these mechanical variables under different structural conditions, thereby providing a comprehensive understanding of the system’s behaviour.

In the diagrams corresponding to these three paintings, we can observe the same trends and phenomena present in the sensitivity study diagrams. This consistency across different case studies reinforces the validity of the observations made during the sensitivity analysis, thereby substantiating the robustness of the chosen modelling techniques and assumptions. It provides further evidence that the mechanical behaviours under investigation are not isolated occurrences but are, in fact, generalizable characteristics of the system.

We must emphasize that the selection of the control points (Table 2, red dots), deliberately distanced from the areas of crossbeam application and consequently from the anchor points and friction zones, enables the acquisition of relatively unaltered data sets – even if some of these effects of crossbeams, anchor points, and friction zones are clearly present in the diagrams. As one approaches these specific zones, the results are markedly influenced by these variables, manifesting evident shear and torsional components that are highly case-sensitive.

Discussion

The two following facts are of utmost importance, especially given their complementary meaning.

Firstly, all the cases analysed, which corroborate several previous studies, clearly show that each of the observed cases – both in the sensitivity study and in the real-world scenarios – provides results markedly different from the others in terms of the panel’s deformations over time, and of the stresses and deformations of the wooden panel and of the paint layers. In other words, we find confirmation that each case is unique and necessitates direct testing on the actual artwork if we aim to obtain analytical results representing accurately its actual physical state.

However, it also emerges that certain general behavioural logics are common for all the cases analysed, irrespective of the hygro-mechanical characteristics of the materials and of the geometric features of the panel. This gives a particular focus to understanding the behaviour of these works of art, i.e. we must recognise that their

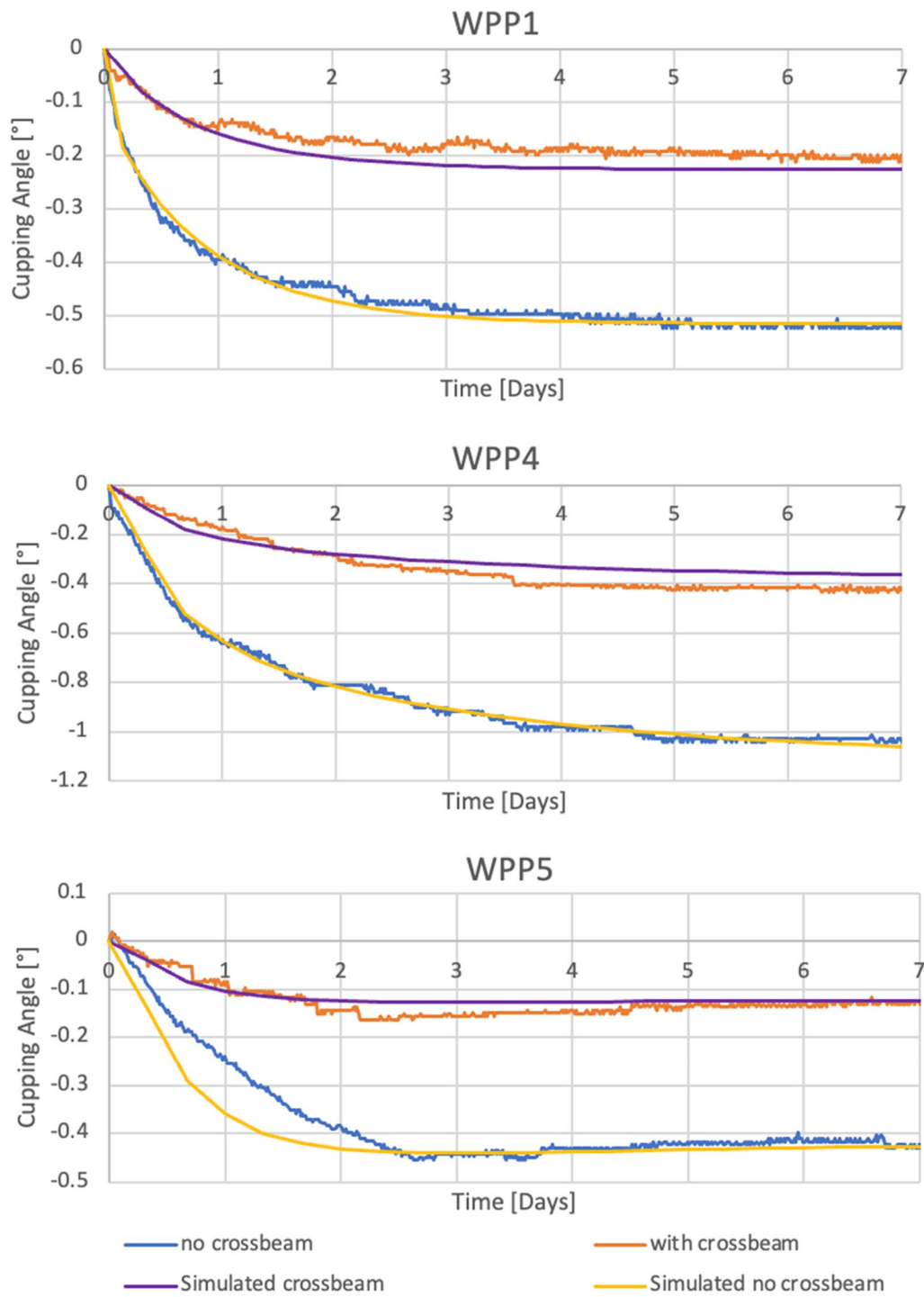


Fig. 9 Comparison between the experimental results and simulations of the panels with and without crossbeams

diversity is inscribed in a constant and, fortunately, simple dynamic of macro-behaviour.

In what follows, we illustrate how different deformation mechanisms arise due to short- and long-term climatic

variations, both with and without crossbeams. In particular, we will focus on how stresses and deformations interact with the paint layers and how they may be concentrated in other topical areas of the sections.

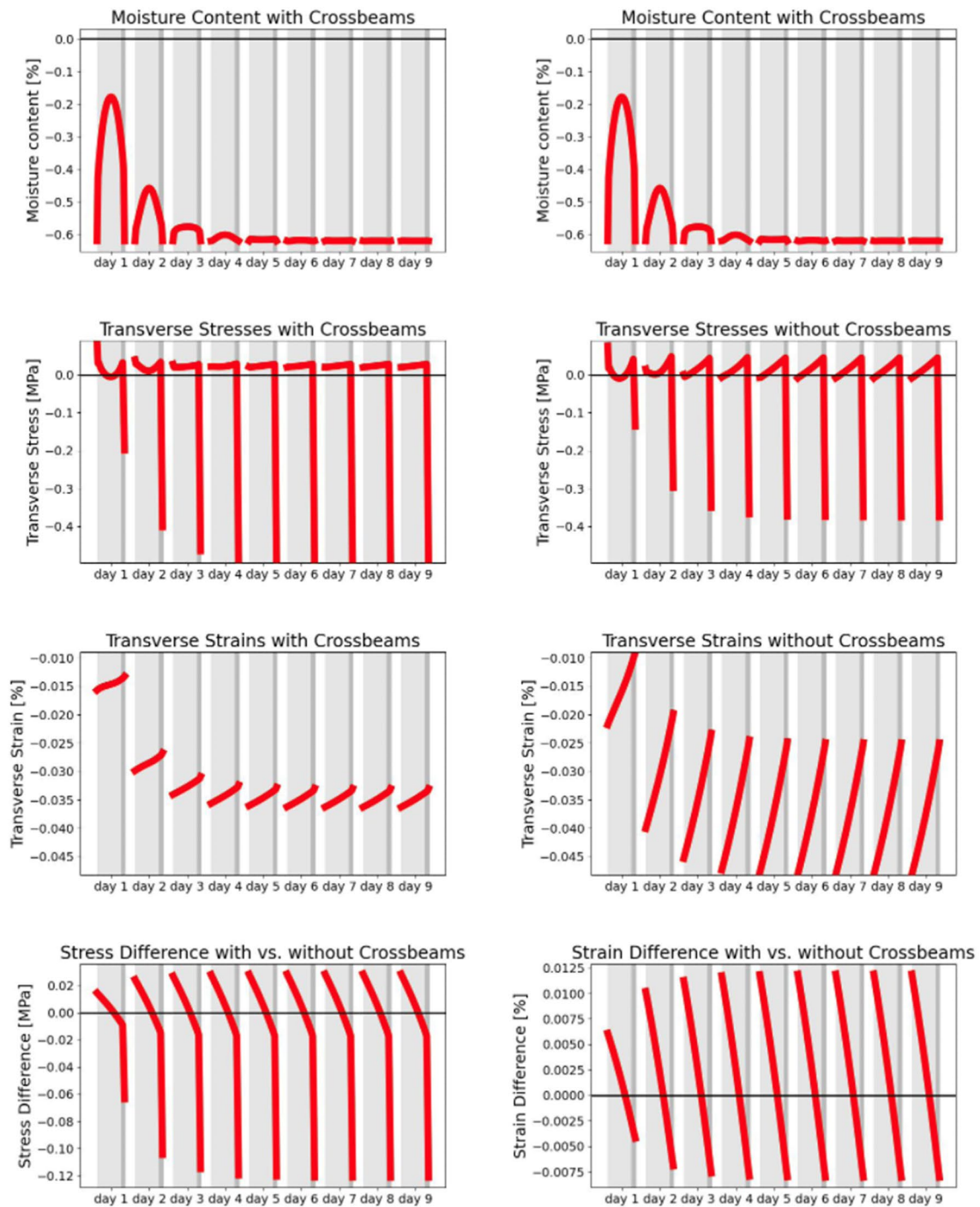


Fig. 10 Results of WPP1 in terms of Moisture content variation from the previous equilibrium state, stresses and strains in the plane of the panel perpendicular to the grain in the cross section for the panel with and without the crossbeams, and the difference in stress and strains between the two states. As the gradient of moisture content in the thickness of the panel is the driver of the phenomenon it is repeated two times in the first row to assure to the reader a vertical responsiveness on both columns and the fact that the distribution of moisture is exactly the same at each timestep for both cases with and without crossbeams

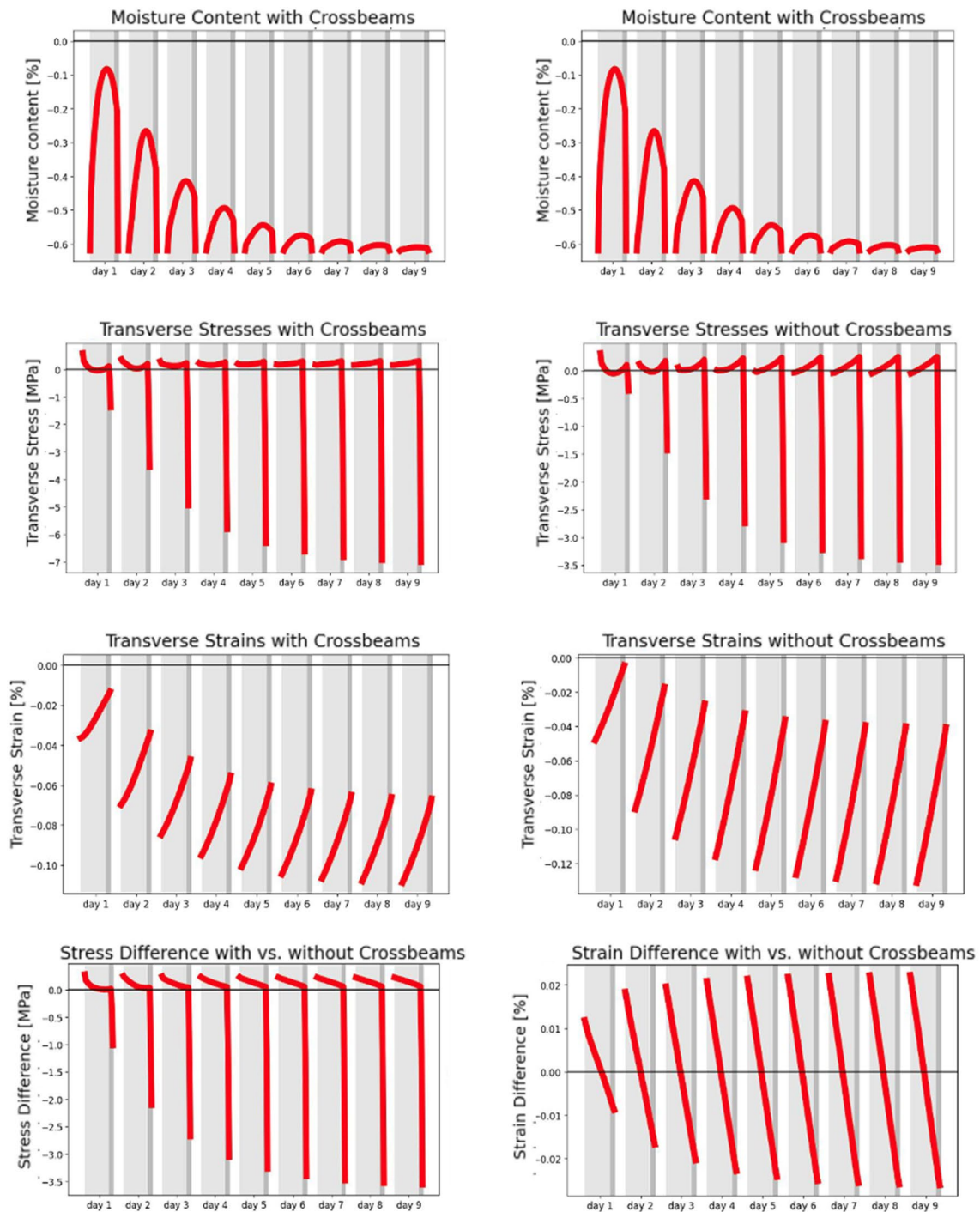


Fig. 11 Results of WPP4 in terms of Moisture content variation from the previous equilibrium state, stresses and strains in the plane of the panel perpendicular to the grain in the cross section for the panel with and without the crossbeams, and the difference in stress and strains between the two states. As the gradient of moisture content in the thickness of the panel is the driver of the phenomenon it is repeated two times in the first row to assure to the reader a vertical resonance on both columns and the fact that the distribution of moisture is exactly the same at each timestep for both cases with and without crossbeams

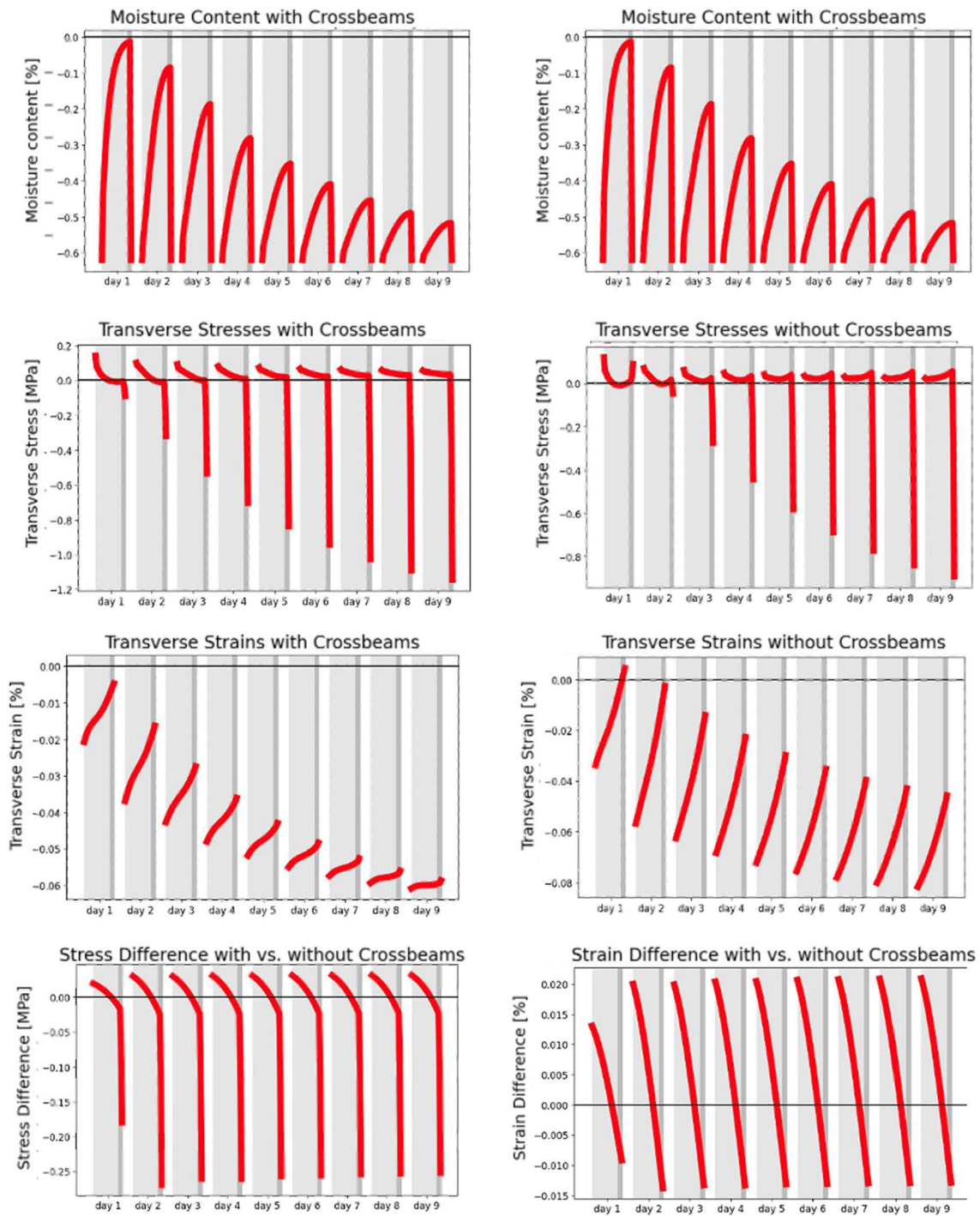


Fig. 12 Results of WPP5 in terms of Moisture content variation from the previous equilibrium state, stresses and strains in the plane of the panel perpendicular to the grain in the cross section for the panel with and without the crossbeams, and the difference in stress and strains between the two states. As the gradient of moisture content in the thickness of the panel is the driver of the phenomenon it is repeated two times in the first row to assure to the reader a vertical response on both columns and the fact that the distribution of moisture is exactly the same at each timestep for both cases with and without crossbeams

The analysis of the diagrams [Figs. 5, 6, 7, 10, 11, 12] leads us to the following considerations regarding the internal behaviour of WPPs:

- **Short-period transients:** In the initial moments of hygroscopic transients, the most stressed part is the back face of the panel. In cases of significant transients occurring over relatively short time spans, such compressive or tensile stresses could potentially lead to fractures (in tension) or plasticization (in compression, thereby originating “compression set”) in the wood layers immediately beneath the back face of the panel.
- **Long-period transients:** As the climatic variation is maintained, the situation reverses, with the paint layers becoming the primary responders to the wood’s deformation tendencies due to their inherent stiffness and strength. Stiff ground layers consequently result in significant accumulations of stress in their interior. This is primarily due to the stiffness difference between the wood and paint layers, as well as the differing hygroscopic properties of these two different layers. This phenomenon becomes particularly relevant in the context of medium to long-term climatic variations—monthly, seasonal, or annual—highlighting that the major consequences of such changes are almost entirely taken up by the paint layers.
- **Main crossbeams behaviours:** The crossbeam primarily exhibits flexural behaviour, which is thus described by a flexural shape diagram in the deformation field. We can safely assume that the dynamics of “flying wood” and “non-flying wood” are not significantly altered by the presence of the crossbeams. The crossbeams contribute primarily in a flexural capacity and do not give a hygroscopic contribution to the system. The asymmetry of this diagram leads us to observe that an axial stress is also present, albeit generally much smaller than the flexural stress, in the transverse direction of the panel. For axial stress is here intended a stress which develops in the panel along the longitudinal axis of the crossbeam. This axial stress originates primarily from three components:
 - The different hygroscopic deformation tendencies between wood and paint layers.
 - The different hygroscopic deformation tendencies between wood and paint layers.
 - The reaction of the connectors, tangential to the plane of the panel, due to the relative movement of the panel and the crossbeams
- The flexural deformation induced by the crossbeam amplifies the deformation in the paint layers, consequently reducing the interaction or coaction between the wood and paint layers.
- **Sectional deformation containment:** The effect of constraining the cupping deformations of the panel, at the sectional level, results in a reduction of strains at the back face and in an increase of strains on the front, painted, face. Correspondingly, there is a slight decrease in stress levels on the back face while a more significant increase is observed on the front painted face.
- **Global containment effect:** In summary, the global containment effect exerted by the crossbeams results in a reduction of the risk of fractures and compression set on the back face of the panel. However, this comes at the expense of increased compression stresses and strains in the paint layers.
- **Zero strain plane:** In the historical WPPs examined, except for the first day for WPP5, all other cases, at any time, show sections that are completely compressed for a moisture decrease. This implies that if the deformability is conceptualised as a uniform transverse shortening deformation combined with a centroidal rotational deformation, their aggregate always results in a complete contraction of the section. If we assume that a zero-strained surface exists, where the deformations are identically zero, we can also assume that each section is rotating around an axis lying on this surface. In the case of simple bending, we understand that the cross section of a beam rotates about its centroid. However, when an axial force is combined with bending, in what is known as press-bending, the point of rotation of the section shifts within the cross-section and may even extend beyond it. There is therefore a specific point of rotation for each section, which for a single beam becomes a line. Consequently, we can conceptualise this locus of points around which a section rotates in a given direction (in our case, transverse) as a 2D surface for our cases. In this context, we can note that only for WPP5, this zero-strain surface is located within the panel only during the first day of climate change when no crossbeams are applied; the identification can be made by the intersection of the red line with the zero deformation value on day 1 in the ‘transverse strain without crossbeams’ graph of Fig. 12. In all other cases it remains outside the panel, on the side of the paint layers.
- **Maximum mechanical interaction:** By ‘maximum mechanical interaction’, we refer to the moment when the painting’s propensity for deformation reaches its

peak, thereby eliciting the maximal response from the crossbeam. Consequently, it is reasonable to surmise, and our models corroborate this, that at this juncture, the greatest interaction forces between the crossbeam and the planking occur. Clearly, this moment, given that the behaviour of the crossbeams is purely flexural, corresponds to the point of maximum stress of the paint layers by the crossbeams. For panels that exhibit a 'flying wood' behaviour, the moment of maximum mechanical interaction between the crossbeam and the panel occurs at the peak of the 'flying wood' phenomenon and is therefore of short duration. This moment is characterised by large internal moisture content gradients. After this moment, the interaction tends to stabilise on smaller values. For panels that exhibit a 'non-flying wood' behaviour, the moment of maximum interaction occurs when the panel is stabilized, that is, when the internal moisture content gradients disappear. We can therefore assert, based on the observed results, that for the paintings WPP1 and WPP4, this condition is realized at a stabilized moisture gradient, typically towards the end of the time-history. In contrast, for WPP5, it develops at the peak of its 'flying wood' behaviour, specifically on day 2.

Up to this point, we have focused on discussing the general findings that have emerged from this research. We now wish to deal with the specific implications for

WPP4 and WPP5, particularly concerning step-change hygroscopic transients and the effects of restraining them with crossbeams. In previous analyses, we selected results from points that are minimally influenced by the boundary conditions of the panel. Now, we aim to correlate transversal strains — i.e. the deformation field perpendicular to the grain—with the overall shape change of the panel at the peak moments of panel-crossbeam interaction. For WPP4 this occurs when internal gradients have ended, whereas for WPP5 this occurs at the peak of the 'flying wood' behaviour.

For WPP4 (Fig. 13), it is immediately evident that without crossbeams it is severely distorted. The deformation tendencies of the boards, originating from their anatomical features, are easily discernible. We can observe that the panel exhibits more pronounced deformations in the central regions of each plank, which are closest to the assumed location of the pith, outside the boards. These are the areas where there is a strong transition between radial and tangential directions within the boards.

Upon examining the panel with crossbeams, we find that it remains contracted throughout, albeit with concentrations of contractions slightly shifted from the centres of the boards, in the direction of the connectors, due to the global flexural effect of the crossbeams. In terms of warping deformations, the crossbeams significantly homogenize the curvature, barely revealing the tendencies of individual boards. The crossbeam serves a crucial mechanical function by shifting the local behaviour of

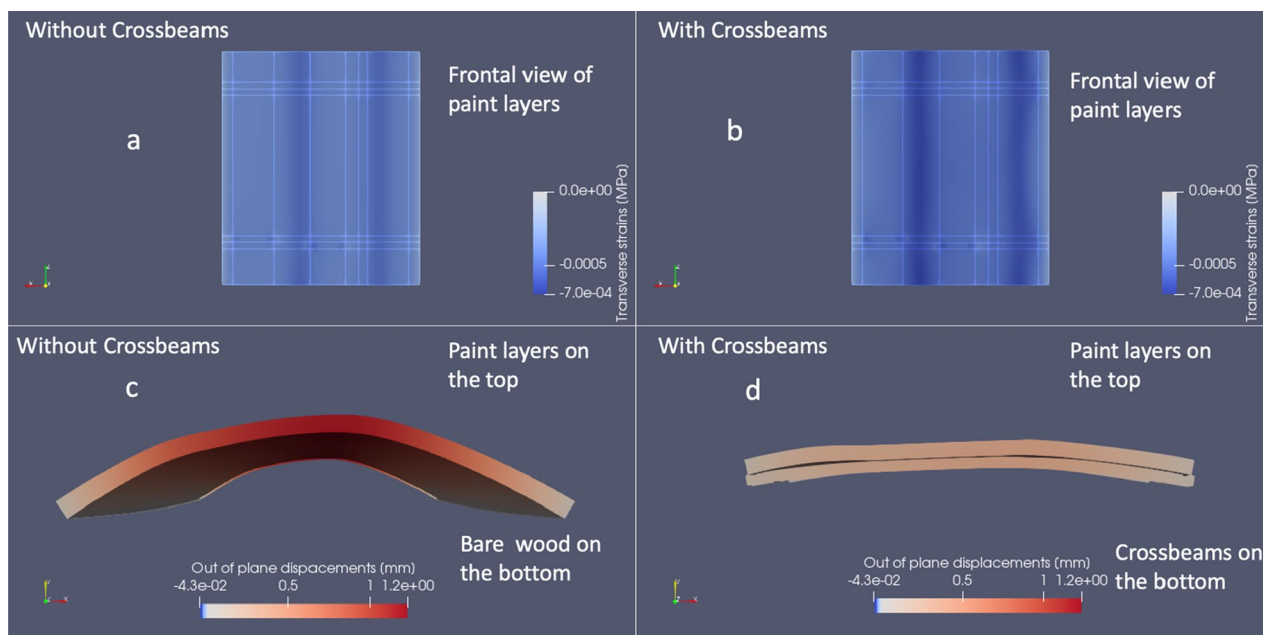


Fig. 13 Mechanical simulated response of WPP4 at the moment of maximum interaction between panel and crossbeams in day 9. a: transverse strain of the paint layers without crossbeams. b: transverse strain of the paint layers with crossbeams. c: out of plane displacements on the artwork without crossbeams seen from its top. d: out of plane displacements on the artwork with crossbeams seen from its top

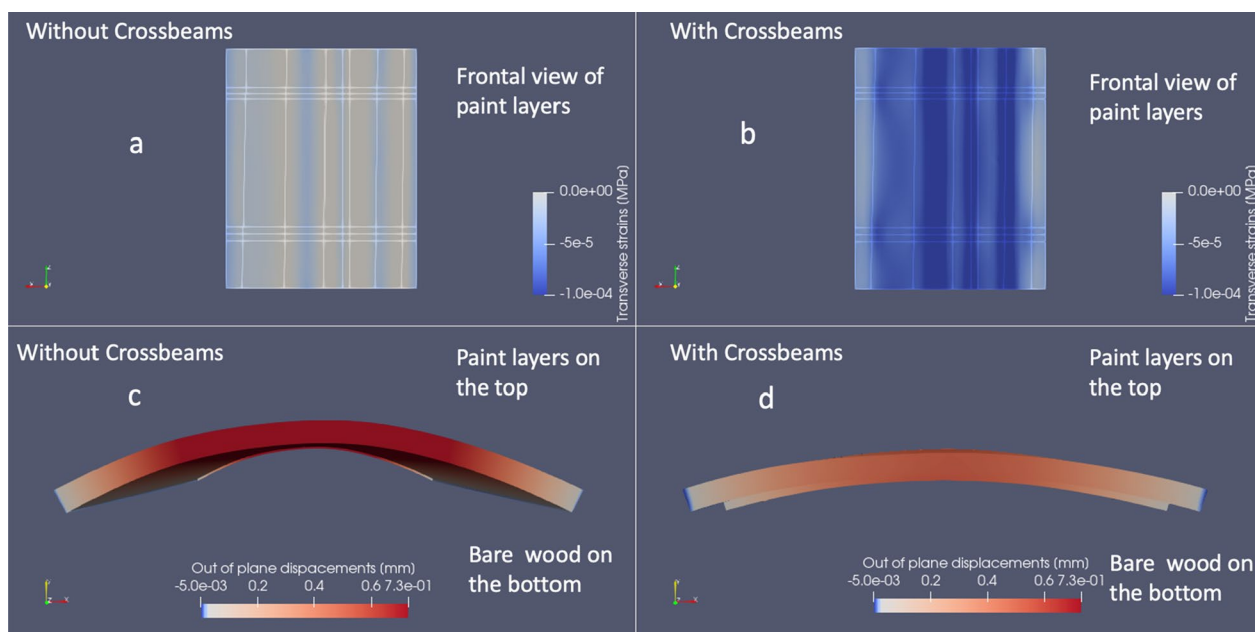


Fig. 14 Mechanical simulated response of WPP5 at the moment of maximum interaction between panel and crossbeams in day 2.. a: transverse strain of the paint layers without crossbeams. b: transverse strain of the paint layers with crossbeams. c: out of plane displacements on the art piece without crossbeams seen from its top. d: out of plane displacements on the art piece with crossbeams seen from its top

individual boards to a global panel behaviour. It redistributes stresses across various boards based on their geometric and mechanical characteristics (Fig. 14).

In the case of WPP5, we observe that the curvature of the panel is considerably more uniform. This uniformity is primarily attributed to the greater thickness of the boards and their increased distance from their assumed location of the pith. From the perspective of deformations in the paint layers, we note that they are generally homogeneously tensile, with peaks of compression observed in the central regions of the boards and in the transition zone between the two boards. Upon transitioning to the condition with crossbeams, their flexural contribution becomes evident in the emergence of alternating tensile and compressive zones. These zones are largely influenced by the areas of anchorage and contact between the crossbeams and the panel boards. In summary, the crossbeams introduce a complex interplay of tensile and compressive stresses, which is most pronounced near the points of anchorage and contact. This highlights the significant role of crossbeams in modulating the mechanical behaviour of WPP5, particularly in terms of stress distribution and deformation characteristics.

Conclusions

This study demonstrates the technical feasibility and critical importance of introducing highly calibrated models based on original WPPs to assess the mechanical state of

an artwork subject to environmental thermo-hygrometric variations. These models, which we have termed "digital twins," have enabled two types of analyses within this two-level study that are both distinct and complementary. On one hand, we identified general and common characteristics applicable to most Wooden Panel Paintings (WPPs), including behaviours for long and short-term variations and the role of crossbeam systems. On the other hand, we conducted specific studies on individual artworks, resulting in a comprehensive and intricate framework that depicts the primary internal dynamics of WPPs, both with and without crossbeams. Integrating this with our previous findings, it becomes evident that while general behavioural logics are common to every case analysed, these are not sufficient for precise analysis of what occurs within a WPP. This brings us to a couple of final reflections.

The first is that although common dynamics have been identified, they are not sufficient for a precise analysis; to move to this level, it is necessary to have a well-calibrated advanced model based on hygroscopic tests, or a "digital twin."

The second and more significant reflection is that the digital twin tool can allow for the analytical evaluation of engineered restoration interventions. For example, it can inform the decision to change or thin the crossbeams, or analyse the consequences of a time-history of temperature and relative humidity on the painting in terms of stresses and deformations. This can enable the evaluation

of museum environments in terms of the well-being of the artworks.

In summary, our study not only contributes to the understanding of the complex interplay of mechanical variables under different structural conditions but also underscores the value of adopt advanced modelling techniques like digital twins for both general and specific analyses. These models serve as a crucial tool for the analytical evaluation of engineered restoration interventions and the well-being of artworks in museum environments.

Annex

In Annex, an elucidation is provided for the interpretation of the graphs in Fig. 15, with the objective of facilitating the reader’s comprehension.

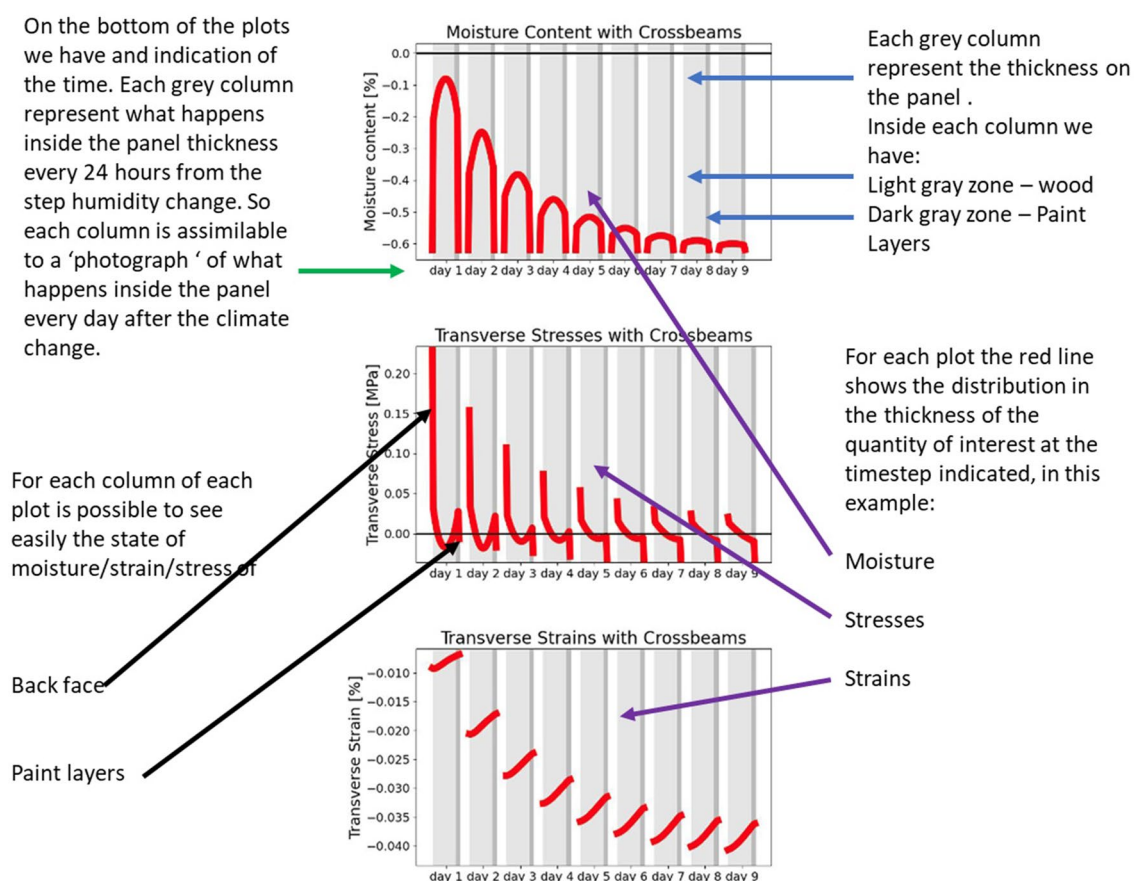


Fig. 15 Explanation on how to read the plots

Supplementary Information

The online version contains supplementary material available at <https://doi.org/10.1186/s40494-023-01106-z>.

Additional file 1: Figure S1. Test 1 -Results in terms of Moisture content, stresses and strains in the plane of the panel perpendicular to the grain in the cross section for the panel with and without the crossbeams, and the difference in stress and strains between the two states. As the gradient of moisture content in the thickness of the panel is the driver of the phenomenon it is repeated two times in the first row to assure to the reader a vertical response on both columns and the fact that the distribution of moisture is exactly the same at each timestep for both cases with and without crossbeams. **Figure S2.** Test 2 -Results in terms of Moisture content, stresses and strains in the plane of the panel perpendicular to the grain in the cross section for the panel with and without the crossbeams, and the difference in stress and strains between the two states. As the gradient of moisture content in the thickness of the panel is the driver of the phenomenon it is repeated two times in the first row to assure to the reader a vertical response on both columns and the fact that the distribution of moisture is exactly the same at each timestep for both cases with and without crossbeams. **Figure S3.** Test 3 -Results in terms of Moisture content, stresses and strains in the plane of the panel perpendicular to the grain in the cross section for the panel with and without the crossbeams, and the difference in stress and strains between the two states. As the gradient of moisture content in the thickness of the panel is the driver of the phenomenon it is repeated two times in the first row to assure to the reader a vertical response on both columns and the fact that the distribution of moisture is exactly the same at each timestep for both cases with and without crossbeams. **Figure S4.** Test 4 -Results in terms of Moisture content, stresses and strains in the plane of the panel perpendicular to the grain in the cross section for the panel with and without the crossbeams, and the difference in stress and strains between the two states. As the gradient of moisture content in the thickness of the panel is the driver of the phenomenon it is repeated two times in the first row to assure to the reader a vertical response on both columns and the fact that the distribution of moisture is exactly the same at each timestep for both cases with and without crossbeams. **Figure S5.** Test 5 -Results in terms of Moisture content, stresses and strains in the plane of the panel perpendicular to the grain in the cross section for the panel with and without the crossbeams, and the difference in stress and strains between the two states. As the gradient of moisture content in the thickness of the panel is the driver of the phenomenon it is repeated two times in the first row to assure to the reader a vertical response on both columns and the fact that the distribution of moisture is exactly the same at each timestep for both cases with and without crossbeams. **Figure S6.** Test 6 -Results in terms of Moisture content, stresses and strains in the plane of the panel perpendicular to the grain in the cross section for the panel with and without the crossbeams, and the difference in stress and strains between the two states. As the gradient of moisture content in the thickness of the panel is the driver of the phenomenon it is repeated two times in the first row to assure to the reader a vertical response on both columns and the fact that the distribution of moisture is exactly the same at each timestep for both cases with and without crossbeams. **Figure S7.** Test 7 -Results in terms of Moisture content, stresses and strains in the plane of the panel perpendicular to the grain in the cross section for the panel with and without the crossbeams, and the difference in stress and strains between the two states. As the gradient of moisture content in the thickness of the panel is the driver of the phenomenon it is repeated two times in the first row to assure to the reader a vertical response on both columns and the fact that the distribution of moisture is exactly the same at each timestep for both cases with and without crossbeams. **Figure S8.** Test 8 -Results in terms of Moisture content, stresses and strains in the plane of the panel perpendicular to the grain in the cross section for the panel with and without the crossbeams, and the difference in stress and strains between the two states. As the gradient of moisture content in the thickness of the panel is the driver of the phenomenon it is repeated two times in the first row to assure to the reader a vertical response on both columns and the fact that the distribution of moisture is exactly the same at each timestep for both cases with and without crossbeams.

Figure S9. Test 9 -Results in terms of Moisture content, stresses and strains in the plane of the panel perpendicular to the grain in the cross section for the panel with and without the crossbeams, and the difference in stress and strains between the two states. As the gradient of moisture content in the thickness of the panel is the driver of the phenomenon it is repeated two times in the first row to assure to the reader a vertical response on both columns and the fact that the distribution of moisture is exactly the same at each timestep for both cases with and without crossbeams. **Figure S10.** Test 10 -Results in terms of Moisture content, stresses and strains in the plane of the panel perpendicular to the grain in the cross section for the panel with and without the crossbeams, and the difference in stress and strains between the two states. As the gradient of moisture content in the thickness of the panel is the driver of the phenomenon it is repeated two times in the first row to assure to the reader a vertical response on both columns and the fact that the distribution of moisture is exactly the same at each timestep for both cases with and without crossbeams. **Figure S11.** Test 11 -Results in terms of Moisture content, stresses and strains in the plane of the panel perpendicular to the grain in the cross section for the panel with and without the crossbeams, and the difference in stress and strains between the two states. As the gradient of moisture content in the thickness of the panel is the driver of the phenomenon it is repeated two times in the first row to assure to the reader a vertical response on both columns and the fact that the distribution of moisture is exactly the same at each timestep for both cases with and without crossbeams. **Figure S12.** Test 12 -Results in terms of Moisture content, stresses and strains in the plane of the panel perpendicular to the grain in the cross section for the panel with and without the crossbeams, and the difference in stress and strains between the two states. As the gradient of moisture content in the thickness of the panel is the driver of the phenomenon it is repeated two times in the first row to assure to the reader a vertical response on both columns and the fact that the distribution of moisture is exactly the same at each timestep for both cases with and without crossbeams.

Acknowledgements

This research received specific grant from Tuscan Region, Italy (PREMUDE Project—POR-FSE 2014–2020. Modelli innovativi per la conservazione PREeventiva in ambienti MUseali e DEpositi temporanei post-emergenza).

Author contributions

LR conceived and discussed the theoretical approach, the methods implemented and the numerical procedures applied, did every step of the modelling, developed the behaviour law of wood, analysed the models and elaborated the conclusions, developed the experimental investigations, wrote and revised the paper. PM developed the experimental investigations, discussed the results and revised the paper. TH developed the behaviour law of wood. CM developed the experimental investigations. LU developed the experimental investigations, discussed and reviewed the conclusions, revised the paper. LR, SR, AS and CC chose and provide the six historical panel paintings, participated in designing the tests, discussed the results and revised the paper. JG discussed the methods implemented, reviewed and discussed the numerical results, revised the paper. MF conceived and discussed the theoretical approach, discussed the methods implemented and the numerical procedures applied, reviewed and discussed the results, revised the paper, coordinated the project. All authors read and approved the final manuscript.

Availability of data and materials

Data are available from the corresponding author [PM.] upon reasonable request and with permission of the Superintendence that owns the panel paintings.

Declarations

Competing interests

The authors declare that they have no known competing financial interests or personal relationships that could have appeared to influence the work reported in this paper.

Received: 13 October 2023 Accepted: 29 November 2023

Published online: 25 January 2024

References

- Uzielli L. Historical overview of panel-making techniques in central Italy. In: Proceedings of a Symposium at the J. Paul Getty Museum 24–28 April 1995. 1998, pp. 110–135
- Wadum J. Historical overview of panel-making techniques in northern countries. In: Proceedings of a Symposium at the J. Paul Getty Museum 24–28 April 1995. 1998, pp. 149–177
- Riparbelli L, Mazzanti P, Manfriani C, Uzielli L, Castelli C, Gualdani G, Ricciardi L, Santacesaria A, Rossi S, Fioravanti M. Hygromechanical behaviour of wooden panel paintings: classification of their deformation tendencies based on numerical modelling and experimental results. *Herit Sci*. 2023;11:25. <https://doi.org/10.1186/s40494-022-00843-x>.
- Riparbelli L, Brémand F, Dionisi-Vici P, Dupré JC, Goli G, Hesser F, Jullien D, Mazzanti P, Togni M, Ravaud E, Uzielli L, Gril J. Learning from objects: the use of advanced numerical methods to exploit a complete set of information from experimental data, for the Mona Lisa's Digital-Twin. *IOP Conf Ser Mater Sci Eng*. 2020;949: 012089. <https://doi.org/10.1088/1757-899X/949/1/012089>.
- Riparbelli L, Dionisi-Vici P, Mazzanti P, Brémand F, Dupré JC, Fioravanti M, Goli G, Helfer T, Hesser F, Jullien D, Mandron P, Ravaud E, Togni M, Uzielli L, Badel E, Gril J. Coupling numerical and experimental methods to characterise the mechanical behaviour of the Mona Lisa: a method to enhance the conservation of panel paintings. *J Cult Herit*. 2023;62:376–86. <https://doi.org/10.1016/j.culher.2023.06.013>.
- Riparbelli L, Mazzanti P, Helfer T, Manfriani C, Uzielli L, Castelli C, Santacesaria A, Ricciardi L, Rossi S, Gril J, Fioravanti M. Modelling of hygro-mechanical behaviour of wooden panel paintings: model calibration and artworks characterisation. *Herit Sci*. 2023;11:126. <https://doi.org/10.1186/s40494-023-00958-9>.
- Gril J, Jullien D, Hunt D. Compression set and cupping of painted wooden panels. In: Analysis and characterisation of wooden cultural heritage by scientific engineering methods. Halle (Saale), Germany, 2016
- Hunt D, Uzielli L, Mazzanti P. Strains in gesso on painted wood panels during humidity changes and cupping. *J Cult Herit*. 2017;25:163–9.
- Rachwał B, Bratasz Ł, Krzemień Ł, Łukowski M, Kozłowski R. Fatigue damage of the gesso layer in panel paintings subjected to changing climate conditions. *Strain*. 2012;48:474–81. <https://doi.org/10.1111/j.1475-1305.2012.00844.x>.
- Bratasz Ł, Vaziri Sereshk MR. Crack saturation as a mechanism of acclimatization of panel paintings to unstable environments. *Stud Conserv*. 2018;63:22–7. <https://doi.org/10.1080/00393630.2018.1504433>.
- Łukowski M. Painted wood. What makes the paint crack? *J Cult Herit*. 2012;13:590–3. <https://doi.org/10.1016/j.culher.2012.01.007>.
- Jullien D, Dupré J-C, Gauvin C, Uzielli L, Hesser F, Riparbelli L, Mazzanti P, Gril J, Tournillon G, Amoroso D, Hazaël-Massieux P, Stepanoff P, Bousvarou M. Hygromechanical study of a 16th century painted wooden panel: In-situ experiments to quantify the mechanical effect of the frame and the cradle. *J Cult Herit*. 2023;64:266–74. <https://doi.org/10.1016/j.culher.2023.10.011>.
- Allegretti O, De Vincenzi M, Uzielli L, Dionisi-Vici P. Long-term hygromechanical monitoring of Wooden Objects of Art (WOA): a tool for preventive conservation. *J Cult Herit*. 2013;14:e161–4. <https://doi.org/10.1016/j.culher.2012.10.022>.
- Dupré J-C, Jullien D, Uzielli L, Hesser F, Riparbelli L, Gauvin C, Mazzanti P, Gril J, Tournillon G, Amoroso D, Massieux PH, Stepanoff P, Bousvarou M. Experimental study of the hygromechanical behaviour of a historic painting on wooden panel: devices and measurement techniques. *J Cult Herit*. 2020;46:165–75. <https://doi.org/10.1016/j.culher.2020.09.003>.
- Gauvin C. Etude expérimentale et numérique du comportement hygromécanique d'un panneau de bois : application à la conservation des tableaux peints sur bois du patrimoine (Experimental and Numerical Study of the Hygromechanical Behavior of a Wooden Panel: Application to the Conservation of Painted Wood Panels in Heritage, in French). PhD, LMGC - Laboratoire de Mécanique et Génie Civil, 2015
- Mecklenburg M, Tumosa C, Erhardt D. Structural response of painted wood surfaces to changes in ambient relative humidity. In: Painted wood: history and conservation, the getty conservation institute. Dorge V and Howlett FC, US, 1998, pp. 464–483
- Mazzanti P, Togni M, Uzielli L. Drying shrinkage and mechanical properties of Poplar wood (*Populus alba* L.) across the grain. *J Cult Herit*. 2012;13:585–9.
- Mazzanti P, Colmars J, Hunt D, Uzielli L. A hygro-mechanical analysis of poplar wood along the tangential direction by restrained swelling test. *Wood Sci Technol*. 2014;48:673–87. <https://doi.org/10.1007/s00226-014-0633-4>.
- Allegretti O, Raffaelli F. Barrier effect to water vapour of early European painting materials on wood panels. *Stud Conserv*. 2008. <https://doi.org/10.1179/sic.2008.53.3.187>.
- Stöcklein J, Konopka D, Grajcarek G, Tietze O, Oertel S, Schulze A, Kaliske M. Hygro-mechanical short-term behaviour of selected coatings: experiments and material modelling on vapour permeability and mechanical properties. *Herit Sci*. 2022;10:141. <https://doi.org/10.1186/s40494-022-00768-5>.
- Janas A, Mecklenburg MF, Fuster-López L, Kozłowski R, Kékicheff P, Favier D, Andersen CK, Scharff M, Bratasz Ł. Shrinkage and mechanical properties of drying oil paints. *Herit Sci*. 2022;10:181. <https://doi.org/10.1186/s40494-022-00814-2>.
- dePolo G, Walton M, Keune K, Shull KR. After the paint has dried: a review of testing techniques for studying the mechanical properties of artists' paint. *Herit Sci*. 2021;9:68. <https://doi.org/10.1186/s40494-021-00529-w>.
- Froidevaux J. Wood and paint layers aging and risk analysis of ancient panel painting. PhD, Université Montpellier II - Sciences et Techniques du Languedoc, 2012
- Dureisseix D, Marcon B. A partitioning strategy for the coupled hygromechanical analysis with application to wood structures of cultural heritage. *Int J Numer Meth Eng*. 2011;88:228–56.
- Gebhard C, Konopka D, Börner A, Mäder M, Kaliske M. Hygro-mechanical numerical investigations of a wooden panel painting from "Katharinenaltar" by Lucas Cranach the Elder. *J Cult Herit*. 2018;29:1–9.
- Riparbelli L, Castelli C, Gualdani G, Ricciardi L, Santacesaria A, Uzielli L, Mazzanti P. An innovative method for dimensioning the crossbeams of an original painted panel, based on mechanical testing, and on numerically modelling its distortion tendency. In: Furferi R, Governi L, Volpe Y, Gherardini F, Seymour K, editors. The future of heritage science and technologies. Cham: Springer International Publishing; 2023. p. 97–112.
- Saft S, Kaliske M. Numerical simulation of the ductile failure of mechanically and moisture loaded wooden structures. *Comp Struct*. 2011;89:2460–70. <https://doi.org/10.1016/j.compstruc.2011.06.004>.
- Bosco E, Suiker ASJ, Fleck NA. Crack channelling mechanisms in brittle coating systems under moisture or temperature gradients. *Int J Fract*. 2020;225:1–30. <https://doi.org/10.1007/s10704-020-00461-3>.
- Rachwał B, Bratasz Ł, Łukowski M, Kozłowski R. Response of wood supports in panel paintings subjected to changing climate conditions. *Strain*. 2012;48:366–74. <https://doi.org/10.1111/j.1475-1305.2011.00832.x>.
- Cocchi L, Marcon B, Goli G, Mazzanti P, Castelli C, Santacesaria A, Uzielli L. Verifying the operation of an elastic crossbar system applied to a panel painting: the *Deposition from the Cross* by an anonymous artist from Abruzzo, sixteenth century. *Stud Conserv*. 2017;62:150–61. <https://doi.org/10.1080/00393630.2015.1137426>.
- Kupczak A, Jędrychowski M, Strojcecki M, Krzemień Ł, Bratasz Ł, Łukowski M, Kozłowski R. HERIE: a web-based decision-supporting tool for assessing risk of physical damage using various failure criteria. *Stud Conserv*. 2018;63:151–5. <https://doi.org/10.1080/00393630.2018.1504447>.
- Dionisi-Vici P, Mazzanti P, Uzielli L. Mechanical response of wooden boards subjected to humidity step variations: climatic chamber measurements and fitted mathematical models. *J Cult Herit*. 2006;7:37–48.
- Mazzanti P, Dionisi-Vici P, Fioravanti M, Cardinali E, Mialhe J, Togni M, Uzielli L, Riparbelli L. The Medusa Parade Shield by Caravaggio: making its structural replica, laboratory testing, and numerically modelling their hygro-mechanical distortion behaviour. In: Furferi R, Governi L, Volpe Y, Gherardini F, Seymour K, editors. The Future of Heritage Science and Technologies. Cham: Springer International Publishing; 2023. p. 219–34.
- Wang P, Ma X, Fei L, et al. When the digital twin meets the preventive conservation of movable wooden artifacts. *Herit Sci*. 2023;11:54. <https://doi.org/10.1186/s40494-023-00894-8>.
- Hermon S, Niccolucci F, Bakirtzis N, Gasanova S. A Heritage Digital Twin ontology-based description of Giovanni Baronzio's "Crucifixion of Christ" analytical investigation. *J Cult Herit*. 2024;66:48–58. <https://doi.org/10.1016/j.culher.2023.11.004>.

36. EDF - Électricité De France Finite element Code_Aster: analyse des Structures et Thermo-mécanique pour des Etudes et des Recherches , 2023
37. Helfer T, Michel B, Proix J-M, Salvo M, Sercombe J, Casella M. Introducing the open-source mfront code generator: application to mechanical behaviours and material knowledge management within the PLEIADES fuel element modelling platform. *Comput Math Appl*. 2015;70:994–1023. <https://doi.org/10.1016/j.camwa.2015.06.027>.
38. EDF - Électricité De France Éléments de contact dérivés d'une formulation hybride continue. 2017; 1–77
39. Ciatti M. Panel painting: technique and conservation of wood supports, Rev. English ed. Edifir, Firenze, 2006
40. Mazzanti P, Riparbelli L, Marcon B, Fabiani G, Togni M, Uzielli L, Castelli C, Santacesaria A. Experimental tests for mechanical properties of wooden 'buttons' used for attaching auxiliary supports behind panel paintings. *IOP Conf Ser Mater Sci Eng*. 2020;949: 012057. <https://doi.org/10.1088/1757-899X/949/1/012057>.
41. Uzielli L, Cocchi L, Mazzanti P, Togni M, Julien D, Dionisi-Vici P. The Deformometric Kit: a method and an apparatus for monitoring the deformation of wooden panels. *J Cult Herit*. 2012;13:94–101.
42. Kekeliak M, Gocál J, Vičan J. Stiffness of carpentry connections—numerical modelling vs experimental test. *Civil Environ Eng*. 2015;11:121–35. <https://doi.org/10.1515/cee-2015-0016>.
43. Forest Products Laboratory. Wood handbook wood as an engineering material. General Technical Report FPL-GTR-282. Madison: U.S. Department of Agriculture, Forest Service, Forest Products Laboratory. 2021, 543

Publisher's Note

Springer Nature remains neutral with regard to jurisdictional claims in published maps and institutional affiliations.